

OXYGEN LINE FORMATION IN LATE-F THROUGH EARLY-K DISK/HALO STARS: INFRARED O I TRIPLET AND [O I] LINES

YOICHI TAKEDA

Institute of Astronomy, The University of Tokyo, Mitaka, Tokyo 181-0015, Japan

takedayi@cc.nao.ac.jp

ABSTRACT

In order to investigate the formation of O I 7771–5 and [O I] 6300/6363 lines, extensive non-LTE calculations for neutral atomic oxygen were carried out for wide ranges of model atmosphere parameters, which are applicable to early-K through late-F halo/disk stars of various evolutionary stages.

Regarding the triplet O I lines in near IR, for which conspicuous non-LTE effects are observed, a useful formula with tabulated numerical coefficients is presented, applicable to evaluating NLTE corrections for given W_λ and atmospheric parameters (T_{eff} , $\log g$, ξ). On the other hand, our calculations lead to the robust conclusion that LTE is totally valid for the forbidden [O I] lines.

Reanalysis of published equivalent-width data of O I 7771–5 and [O I] 6300/6363 taken from various literatures confirmed that, while a reasonable consistency of O I and [O I] abundances was observed for disk stars ($-1 \lesssim [\text{Fe}/\text{H}] \lesssim 0$), the existence of a systematic abundance discrepancy was confirmed between O I and [O I] lines in conspicuously metal-poor halo stars ($-3 \lesssim [\text{Fe}/\text{H}] \lesssim -1$) without being removed by our non-LTE corrections, i.e., the former being larger by ~ 0.3 dex at $-3 \lesssim [\text{Fe}/\text{H}] \lesssim -2$.

Inspecting the parameter-dependence of this discordance, we suspect that [O I] lines may be weakened by some effect possibly dependent upon the surface gravity, rather than attributing the cause of errors to the side of O I lines.

This interpretation naturally suggests the preference of the “rising” tendency to the “flat” trend as the [O/Fe] ratio of halo stars toward a very metal-poor regime.

Subject headings: line: formation — radiative transfer — stars: abundances — stars: atmospheres — stars: Population II

1. INTRODUCTION

Oxygen abundance determination in F–K stars is one of the most controversial and interesting topics in stellar spectroscopy, especially concerning the behavior of the [O/Fe] ratio in metal-poor halo stars (see, e.g., Carretta et al. 2000; King 2000; Israelian et al. 2001; and the references therein).

Namely, we are faced with a problem currently in hot controversy on the observational side, which stems from the fact that each of the different groups of spectral lines, (a) high-excitation permitted O I lines (e.g., 7773 triplet), (b) low-excitation forbidden [O I] lines (6300/6363 lines), and (c) OH lines at UV ($\sim 3100\text{--}3200 \text{ \AA}$), do not necessarily yield reasonably consistent oxygen abundances in metal-poor stars.

More precisely, a distinct discrepancy is occasionally reported between the abundances derived from O I and [O I] lines in the sense that the former tend to yield systematically higher oxygen abundances than the latter in metal-poor stars (see, e.g., Cavallo et al. 1997), in contrast to the relation between O I and OH lines which give more or less consistent abundances (e.g., Boesgaard et al. 1999). As a result, different trends of O-to-Fe ratio, an important tracer of early nucleosynthesis in our Galaxy, have naturally been suggested: (1) plateau-like [O/Fe] from [O I] lines, and (2) ever-rising [O/Fe] from O I or OH lines.

Admittedly, what has been described above is nothing but a rough summary and the actual situation is more complicated than such a simple dichotomic picture. For example, according to the recent investigation of Caretta et al. (2000), a flat [O/Fe] trend was concluded consistently from *both* of the O I and [O I] lines. In addition, the O I vs. [O I] discordance appears to be observed only in *metal-poor* halo stars, since such a systematic disagreement is absent in population I G–K giants (cf. Takeda et al. 1998)

This confusion makes us wonder which on earth is the correct and reliable indicator of the oxygen abundance. Generally speaking, a modest view currently preferred by many people is that [O I] lines are less problematic and more creditable due to their weak T_{eff} sensitivity as well as the general belief of the validity for the assumption of LTE, while O I and OH lines are less reliable (in spite of the abundances derived therefrom are nearly in agreement) because of the uncertainties involved with the non-LTE correction (O I) or with the effect of atmospheric inhomogeneity (OH).

Recently, however, we cast doubt on this conservative picture and suggested the possibility of erroneously underestimated abundances from [O I] lines (i.e., the problem may be due to the formation of forbidden lines rather than that of permitted lines) based on our analysis of seven very metal-poor stars (Takeda et al. 2000), which indicated the tendency of above-mentioned O I vs. [O I] discrepancy (though a small number of sample stars prevented us from making any convincing argument).

Motivated by that work suggesting the necessity of a follow-up study to check if our hypothesis is reasonable or not, we decided to revisit this O I vs. [O I] problem while paying special attention to the topic of the non-LTE correction to be applied, one of the controversial factors in oxygen abundance determination. Toward this aim, we carried out new extensive non-LTE calculations, based on which the numerous published equivalent-width data were reanalyzed to derive the non-LTE abundances, in order to discuss whether or not the abundance discrepancy between O I and [O I] really exists, which we hope to shed some light on the oxygen problem of metal-deficient stars mentioned above.

The purpose of this paper is summarized into the following four points:

- First, extensive tables of non-LTE corrections for the O I 7771–5 triplet lines over a wide range of atmospheric parameters are presented, so that they may be applied to late-F through early-K dwarfs/giants of various metallicities.
- Second, in order for application of such tables to actual analysis of observational data, we try to find out a useful analytical formula for evaluating non-LTE corrections of these O I triplet lines for any given atmospheric parameters (T_{eff} , $\log g$, ξ) and an observed equivalent width (W_λ).
- Third, we investigate the possibility of a non-LTE effect for the low-excitation forbidden [O I] 6300/6363 lines, for which few such attempt has ever been made.
- Fourth, equivalent-width data of O I 7771–5 lines as well as [O I] 6300/6363 lines taken from various literatures are reanalyzed within the framework of the consistent system of analysis along with application of our non-LTE correction formula, in order to discuss the characteristics of [O/Fe] vs. [Fe/H] relation derived from permitted O I lines and forbidden [O I] lines separately.

Also, as a supplementary subject related to this study, the influence of the treatment of H I collision on the non-LTE corrections of O I 7771–5 lines was quantitatively estimated, and the consistency of the present choice of this parameter was checked by comparing the abundances of nearby solar-type stars derived from O I 7771–5, O I 6158, and [O I] 6300 lines. In addition, we tried to explain the W_λ -dependence of the NLTE corrections for O I 7771–5 in terms of the simple two-level-atom model, which gives us an insight to understanding the mechanism of formation for these triplet lines. These are separately described in Appendices A and B, respectively.

2. STATISTICAL EQUILIBRIUM CALCULATIONS

2.1. Atomic Model

The procedures of our non-LTE calculations for neutral atomic oxygen are almost the same as those described in Takeda (1992), which should be consulted for details. We only mention here that the calculation of collision rates in rate equations basically follows the recipe described in Takeda (1991). Especially, the effect of H I collisions, an important key factor in the non-LTE calculation of F–K stars, was treated according to Steenbock & Holweger’s (1984) classical formula *without any correction* as has been done in our oxygen-related works so far, which we believe to be a reasonable choice as far as our calculations are concerned (cf. Takeda 1995, and Appendix A).

There is, however, an important change concerning the atomic model as described below. The model oxygen atom adopted in Takeda (1992) was constructed mainly based on the atomic data (energy level data and gf values) compiled by Kurucz & Peytremann (1972), with ~ 30 additional radiative transitions which were missing in their compilation [e.g., resonance transitions whose transition probabilities were taken from Morton (1991)]. This old model did not include the $2s^2\ 2p^4\ ^3P-2p^4\ ^1D$ transition (corresponding to [O I] 6300/6363 lines) explicitly as the radiative transition (i.e., it was treated as if being completely radiatively forbidden in spite of its actually weak connec-

tion), simply because it was not contained in Kurucz & Peytremann (1972). We also noticed that several important UV radiative transitions originating upward from the $2p^4\ ^1D$ term (i.e., upper term of [O I] 6300/6363) were also missing in that old model atom for the same reason.

We, therefore, newly reconstructed the model oxygen atom exclusively based on the data of Kurucz & Bell (1995), with additional transition probability data for $2p^4\ ^1D$ – $3s\ ^3S^\circ$ and $2p^4\ ^1D$ – $3s\ ^5S^\circ$ transitions taken from Vienna Atomic Line Database (VALD; Kupka et al. 1999). Regarding the collisional rate C_{1-2} for the [O I] transition ($2s^2\ 2p^4\ ^3P$ – $2p^4\ ^1D$) mentioned above, the cross-section given in Osterbrock (1974) were used for evaluating the electron collision rates (C_{1-2}^e), and the H I collision rates (C_{1-2}^H) were estimated by scaling C_{1-2}^e (cf. Takeda 1991). The resulting atomic model comprises 87 terms and 277 radiative transitions, which is similar to the old one in terms of the complexity but must be significantly improved, especially for studying the formation of [O I] lines (i.e., more realistic treatment of the 1–2 interaction and the inclusion of as many UV transitions connecting to the upper term 2 as possible).

2.2. Model Atmospheres

We planned to make our calculations applicable to stars from near-solar metallicity (population I) down to very small metallicity (extreme population II) at late-F through early-K spectral types in various evolutionary stages (i.e., dwarfs, subgiants, giants, and supergiants). We, therefore, decided to carry out non-LTE calculations on the extensive grid of one hundred ($5 \times 5 \times 4$) model atmospheres resulting from combinations of five T_{eff} values (4500, 5000, 5500, 6000, 6500 K), five $\log g$ values (1.0, 2.0, 3.0, 4.0, 5.0), and four metallicities (represented by [Fe/H]) (0.0, -1.0 , -2.0 , -3.0). As for the stellar model atmospheres, we adopted Kurucz’s (1993) ATLAS9 models corresponding to the microturbulent velocity (ξ) of 2 km s^{-1} .

2.3. Oxygen Abundance and Microturbulence

Regarding the oxygen abundance used as an input value in non-LTE calculations, we assumed $\log \epsilon_{\text{O}}^{\text{input}} = 8.93 + [\text{Fe}/\text{H}] + [\text{O}/\text{Fe}]$, where $[\text{O}/\text{Fe}] = 0.0$ for the solar metallicity models ($[\text{Fe}/\text{H}] = 0$) and $[\text{O}/\text{Fe}] = +0.5$ for the other metal-deficient models ($[\text{Fe}/\text{H}] = -1, -2, \text{ and } -3$). Namely, the solar oxygen abundance of 8.93 (Anders, Grevesse 1989) was adopted for the normal-metal models, while metallicity-scaled oxygen abundance plus 0.5 dex (allowing for the characteristics of α element) was assigned to the metal-poor models.

The microturbulent velocity (appearing in the line-opacity calculations along with the abundance) was assumed to be 2 km s^{-1} , to make it consistent with the model atmosphere.

3. NON-LTE CORRECTIONS

3.1. Evaluation Procedures

Here, we describe how the non-LTE abundance corrections are evaluated after the departure coefficients, $b \equiv n_{\text{NLTE}}/n_{\text{LTE}}^*$, have been established by statistical equilibrium calculations.

For an appropriately assigned oxygen abundance (A^a) and microturbulence (ξ^a), we first calculated the non-LTE equivalent width (W^{NLTE}) of the line by using the computed non-LTE departure coefficients (b) for each model atmosphere. Next, the LTE (A^L) and NLTE (A^N) abundances were computed from this W^{NLTE} while regarding it as if being a given observed equivalent width. We can then obtain the non-LTE abundance correction, Δ , which is defined in terms of these two abundances as $\Delta \equiv A^N - A^L$.

Strictly speaking, the departure coefficients [$b(\tau)$] for a model atmosphere correspond to the oxygen abundance and the microturbulence of $\log \epsilon_{\text{O}}^{\text{input}}$ and 2 km s^{-1} adopted in the calculations (cf. §2.3). Nevertheless, considering the fact that the departure coefficients (i.e., *ratios* of NLTE to LTE number populations) are (unlike the population itself) not much sensitive to small changes in atmospheric parameters, we applied such computed b values also to evaluating Δ for slightly different A^a and ξ^a from those fiducial values assumed in the statistical equilibrium calculations. Hence, we evaluated Δ for three A^a values ($\log \epsilon_{\text{O}}^{\text{input}}$ and ± 0.3 dex perturbation) as well as three ξ values (2 km s^{-1} and $\pm 1 \text{ km s}^{-1}$ perturbation) for a model atmosphere using the same departure coefficients.

3.2. Results of Computed Corrections

The computation of Δ values was carried out for five lines: three O I lines of 7771–5 triplet and two [O I] lines of 6300/6363 doublet. We used the WIDTH9 program written by R. L. Kurucz for calculating the equivalent width for a given abundance, or inversely evaluating the abundance for an assigned equivalent width. The adopted line data are summarized in Table 1.

Here we give only the $\xi = 2 \text{ km s}^{-1}$ results for O I 7774.17 (the middle line of the triplet) in Table 2.¹ Note that, in contrast to the case of permitted O I line,

As will be described in §4.2, the Δ values for the forbidden [O I] 6300/6363 line turned out to be essentially equal to zero, suggesting the firm validity of LTE.

The complete tables ($\xi = 1, 2, \text{ and } 3 \text{ km s}^{-1}$ results for each of the three triplet lines at

¹The non-LTE corrections for another line, O I 6158, are also given (for the $\xi = 2 \text{ km s}^{-1}$ case on the $[\text{Fe}/\text{H}] = 0$ and -1 models) in Table 7 for the discussion in Appendix A.

7771.94, 7774.17, and 7775.39 Å) are electronically downloadable from the following anonymous ftp site, where the related tables of the numerical coefficients for practical application (cf. §3.3) and a small Fortran program (o74nltec.f) for the user’s convenience are also available.

ftp://www.ioa.s.u-tokyo.ac.jp
 (IP address: 133.11.160.242)
 directory: /Users/takeda/oxygen_fkstars/

3.3. Analytical Formula for Practical Application

It is necessary for us evaluate the non-LTE corrections corresponding to actual equivalent-width data for stars having a wide variety of atmospheric parameters (T_{eff} , $\log g$, ξ) and metallicity ($[\text{Fe}/\text{H}]$), in order to compare them with those derived by others, or to apply them to reanalysis of published data. However, since the raw tabulated values given for each of the individual models (e.g., Table 2) are not necessarily convenient for such practical applications, it is desirable to develop a useful formula for this purpose.

This motivation reminded us of the simple unique correlation between $W_\lambda(\text{O I } 7774.17)$ and its NLTE correction in metal-poor solar-type dwarfs ($5500 \text{ K} \leq T_{\text{eff}} \leq 6500\text{K}$, $3.5 \leq \log g \leq 4.5$, and $-2 \leq [\text{Fe}/\text{H}] \leq 0$) discussed in Takeda (1994; cf. Fig. 10 therein).² If such a relation really holds also in the present case irrespective of the atmospheric parameters (much wider range than that in Takeda 1994), it would greatly simplify our task. However, according to the Δ vs. W^{NLTE} relation for O I 7774.17 depicted in Figure 1 (based on the data in Table 2), the situation is not such simple; i.e., Δ is not only a function of W^{NLTE} but also more or less dependent on T_{eff} and $\log g$ (and ξ). Nevertheless, a close examination revealed that for given T_{eff} , $\log g$, and ξ , the extent of the non-LTE correction (Δ) is a nearly monotonic function of the equivalent width (W_λ) *irrespective of the metallicity* ($[\text{Fe}/\text{H}]$), and that

$$\Delta = a10^{bW_\lambda}, \quad (1)$$

(where W_λ is measured in mÅ) is a very good approximation for an appropriately chosen set of (a, b) , as far as the line is not too strong (i.e., $W_\lambda \lesssim 100\text{mÅ}$).

We therefore determined the best-fit coefficients (a, b) for each combination of $(T_{\text{eff}}, \log g, \xi)$, which are summarized in Tables 4–6 for the O I triplet lines at 7771.94, 7774.17, and 7775.39 Å, respectively.

Practically, we first evaluate (a, b) by interpolating this table in terms of T_{eff} , $\log g$ and ξ of a star in consideration, which are then applied to equation (1) with the observed equivalent width to

²This tendency can be interpreted as being due to the close connection between the extent of the dilution of the line source function (determining the extent of the non-LTE effect) and the strength of these triplet lines (cf. §4.2 in Takeda 1994).

obtain the non-LTE correction.

In order to demonstrate the applicability of this formula, we show the error of equation (1) (defined as $\delta_{\text{error}} \equiv \Delta^{\text{formula}} - \Delta^{\text{actual}}$) as a function of W_λ for the case of O I 7774.17 in Figure 2 (compare it with Figure 1), where we can see that an accuracy within a few hundredths dex is accomplished as far as $W_\lambda \lesssim 100$ mÅ.

4. DISCUSSION

4.1. NLTE Correction for O I Triplet: Comparison with Others

It is interesting to compare the non-LTE corrections for the O I 7771–5 reported in several published studies with those estimated following the procedure described in §3.3 while using the same observational equivalent widths along with the same T_{eff} , $\log g$ and ξ as given in the literature. If W_λ values for two or three lines of the triplet are available, we computed the corrections for each of the lines and their average was used for the comparison.

4.1.1. Takeda et al. (1998, 2000)

Comparisons with the results of our own previous work, Takeda et al. (1998, 2000), are shown in Figures 3a and b.

The non-LTE corrections for O I 7771.94 given in Table 2 of Takeda et al.’s (1998) population I G–K giants analysis are in good agreement with those derived from our approximate formula [Equation (1)], in spite of the fact that extrapolating Table 3 was necessary for stars with ($4250 \text{ K} \lesssim T_{\text{eff}} < 4500 \text{ K}$).

We can also see that the Δ values of O I 7771–5 for very metal-poor giants computed by Takeda et al. (2000) are reasonably consistent with those estimated by the procedure proposed in this study. Note, however, that a somewhat large discrepancy is observed in the $\xi = 5.1 \text{ km s}^{-1}$ case for HD 184266, where two different ξ values were suggested depending on the lines (O I triplet lines and Fe I lines) used for its determination. This indicates that we should be careful at extrapolating Tables 4–6 to considerably outside of the range they cover (e.g., $1 \text{ km s}^{-1} \leq \xi \leq 3 \text{ km s}^{-1}$).

Generally speaking, as far as the O I 7771–5 triplet lines are concerned, the results of our new calculations reported in this paper (e.g., Table 2) are essentially equivalent to our previous studies, in spite of the use of updated new atomic model in connection with the [O I] transition (cf. §2.1). This can be verified also by comparing Table 2 in this paper with Table 7 of Takeda (1994), both of which are practically equivalent. Taking this fact into consideration, we can again confirm from the coincidence shown in Figures 3a and b that Equation (1) with Tables 3–5 is sufficiently accurate and useful for practical applications.

4.1.2. *Tomkin et al. (1992) and Mishenina et al. (2000)*

In Tomkin et al.’s (1992) extensive analysis of C and O abundances in (from mildly to very) metal-deficient dwarfs, they performed non-LTE calculations by using a 15 levels/22 lines atomic model while adjusting the H I collision rate by the requirement that the solar O I 7771–5 lines yield the abundance of 8.92 with the solar model atmosphere of Holweger & Müller (1974). As shown in Figure 4a, the extents of their Δ values ($\lesssim 0.1$ dex) are appreciably smaller than ours.

Comparing our Δ values with the recent non-LTE calculation of Mishenina et al. (2000), who used an atomic model comprising 75 levels/46 transitions and Steenbock & Holweger’s (1984) H I collision formula with a reduction factor of 1/3, we can see that both are in reasonably good agreement in spite of a mild difference in the treatment of H I collision rates (cf. Figure 4b).

4.1.3. *Carretta et al. (2000)*

It is most interesting to compare our Δ values with those adopted by Carretta et al. (2000), who reanalyzed the published $W_\lambda(\text{O I } 7771\text{--}5)$ data of Tomkin et al. (1992) and Edvardsson et al. (1993) and showed that their (NLTE-corrected) O I abundances are consistent with those of [O I] resulting from their reanalysis of $W_\lambda([\text{O I}] 6300/6363)$ data of Sneden et al. (1991) and Kraft et al. (1992). Their corrections are based on Gratton et al.’s (1999) NLTE calculations, where they adopted a model oxygen atom of 13 levels/28 transitions and a mild *enhancement* factor of ~ 3 (determined by the requirement of O I 7771–5/O I 6158 consistency in RR Lyr variables) applied to classical H I collision rates.

In Figure 5a, Carretta et al.’s (2000) NLTE corrections are compared with our corresponding Δ values, which were evaluated from the $W_\lambda(\text{O I } 7771\text{--}5)$ data of Tomkin et al. (1992) and Edvardsson et al. (1993) while adopting the T_{eff} and $\log g$ values used by Carretta et al. (2000) to make the comparison as consistent as possible. An interesting tendency is observed in this figure. That is, while the extents of their non-LTE corrections for Edvardsson et al.’s (1993) F–G disk dwarfs are systematically smaller than ours, this trend disappears and a good agreement is seen in the case of Tomkin et al.’s (1992) considerably metal-poor halo dwarf stars (their $|\Delta|$ values are even larger for two stars).

A closer inspection revealed that this is nothing but the metallicity dependence, as shown in Figure 5b. Namely, their corrections (in terms of the absolute values) are smaller than ours for mildly metal-deficient disk stars ($-1 \lesssim [\text{Fe}/\text{H}] \lesssim 0$), nearly the same for typical halo stars ($-2 \lesssim [\text{Fe}/\text{H}] \lesssim -1$), and eventually become larger than our values for very metal-poor halo stars ($-3 \lesssim [\text{Fe}/\text{H}] \lesssim -2$).

This tendency can be understood also by examining Table 10 of Gratton et al. (1999). We plotted their Δ vs. $W_\lambda(7771.94)$ relations computed for the $\log g = 3.0$ models of different metallicity in Figures 6a and b, each corresponding to $T_{\text{eff}} = 5000$ K and 6000 K, where our correlation

curves [i.e., Equation (1) with the coefficients taken from Table 3] are overplotted. It can be seen from Figure 6a that their Δ values are appreciably smaller than ours for the $T_{\text{eff}} = 5000$ K case, while the strong metallicity-dependence mentioned above is evidently observed for the case of $T_{\text{eff}} = 6000$ K in Figure 6b, which explains the systematic [Fe/H]-dependent difference in Δ between ours and theirs in Figure 5b.

We have thus recognized that (for given T_{eff} and $\log g$) the non-LTE corrections of the Padova group depend not only W_λ but also strongly on [Fe/H], which markedly contradicts our results indicating a unique monotonic function of W_λ irrespective of the metallicity. Although we can not decide confidently which is correct, we feel that their results are dubious, simply because physically reasonable explanations appear to be lacking why the extent of the non-LTE correction increases with a decrease in the metallicity. Let us consider some possibilities, for example:

— If only electron collisions are involved, a lowered metallicity may lead to an enhancement of the non-LTE effect because of a decrease in the electron density as well as in collision rates (see, e.g., Kislman 1991). Actually, however, H I collisions (which they included even with an enhancement factor of ~ 3) are of overwhelming importance compared to electron collisions and are practically independent on the metallicity.

— The UV ionizing radiation field, which conspicuously depends on the metallicity, does not play such an essential role as in other species, because the O I/O II ionization balance is determined (nearly in LTE) by very efficient charge-exchange reactions with H I atoms.

We thus regard it difficult to explain why the lowered metallicity can enhance the extent of the non-LTE effect. In fact, this is just the opposite to what our calculation suggests, since the essential factor affecting the dilution of the line source function is the strength of the relevant line which decreases with a lowered oxygen abundance according to the decrease in the metallicity (cf. §4.2 in Takeda 1994). Curiously, however, an inspection of Gratton et al’s (1999) Fig. 6 suggests that their non-LTE departure coefficients behave themselves consistently with our computational results (see, e.g., Fig. 9 of Takeda 1994); that is, for the case of $T_{\text{eff}} = 6000$ K and $\log g = 4.5$, the departure from LTE is larger for the [Fe/H] = 0 model than for the [Fe/H] = -2 model. In other words, their non-LTE calculations appears quite reasonable in this respect. Then, how could their calculations lead to the tendency of enhanced Δ with a lowered [Fe/H] ?

Anyway, it appears to us that Carretta et al.’s (2000) non-LTE corrections, which are based on the calculations of Gratton et al. (1999), are questionable. This has an important affection: The success of Carretta et al. (2000) in accomplishing the reasonable consistency between O I and [O I] abundances must be mostly due to this tendency that the extent of their non-LTE corrections systematically increases toward a lower [Fe/H]. If such corrections turned out to be dubious, their consequence would have to be reconsidered.

4.2. Validity of LTE for the [O I] 6300/6363 Lines

As mentioned in §1, the search for the possibility of the non-LTE effect in the [O I] lines, based on the new (more realistic) O I atom, was actually one of the main aims in this paper.

According to the present calculation, however, the departure coefficients of the lower term ($2s^2 2p^4 \ ^3P$; hereinafter referred to as “term 1”) and the upper term ($2p^4 \ ^1D$; hereinafter “term 2”) for the [O I] 6300/6363 lines turned out to be essentially equal to unity over almost all atmospheric layers, which guarantees the validity of the assumption of LTE for these forbidden [O I] lines.

The reason for this is attributed to the fact that (1) the population of the lower ground term is thermalized relative to the continuum (i.e., accomplishment of LTE population) owing to the efficient charge-exchange reaction with H atoms, and (2) these lower and upper terms are strongly coupled with collisions which equalize the b values of these two terms.

It was further found after several test calculations that this is a rather robust conclusion, which may not be affected by any uncertainty in the adopted collisional cross section. That is, although little is known and considerable ambiguities are involved in the collisional rates due to H I atoms for this 1–2 transition (C_{1-2}^H ; for which we used the scaled value estimated from C_{1-2}^e), we obtained essentially the same results *even if C_{1-2}^H was completely neglected*; i.e., only the C_{1-2}^e itself is sufficiently large to bring the b values of terms 1 and 2 into the same value of unity.

We also carried out a simulation for the limiting test case of completely neglecting the collisional interaction between terms 1 and 2 ($C_{1-2}^e = C_{1-2}^H = 0$). In this case, an appreciable overpopulation in the upper term 2 was observed (the extent of its NLTE departure growing toward the shallower layer) as a result of the downward cascade via the UV transitions connecting to term 2, which makes the NLTE line strength somewhat smaller compared to the LTE value (i.e., a positive correction in terms of Δ defined in §3.1) because of the resulting inequality of $S_L/B > 1$ in the upper layer. Even in such an extreme case, however, the extent of the computed Δ value is $\lesssim 0.05$ dex in most range of the atmospheric parameters and definitely insignificant in the practical sense. Accordingly, we can confidently conclude that the non-LTE effect can be safely neglected for the [O I] lines, for which LTE must be a valid approximation.

4.3. [O/Fe] vs. [Fe/H] Relation

4.3.1. Procedure of Reanalysis

Now we are ready to study the [O/Fe] vs. [Fe/H] relation of metal-poor stars by reanalyzing the published equivalent-width data of O I 7771/7774/7775 and [O I] 6300/6363 lines while applying the non-LTE corrections based on our calculations.

We adopted the same T_{eff} , $\log g$, [Fe/H], and ξ values as those used in the literatures, from which the data of equivalent widths were taken. Regarding the model atmospheres, we used Kurucz’s

(1993) grid of ATLAS9 models ($\xi = 2 \text{ km s}^{-1}$) which were interpolated with respect to T_{eff} , $\log g$, and $[\text{Fe}/\text{H}]$ of a star. As in §3.2, Kurucz’s WIDTH9 program was invoked for determining the LTE abundance ($\log \epsilon_{\text{O}}^{\text{LTE}}$) while using the line data given in Table 1. Then, the $[\text{O}/\text{Fe}]$ ratio is obtained as

$$[\text{O}/\text{Fe}] \equiv (\log \epsilon_{\text{O}}^{\text{LTE}} + \Delta - 8.93) - [\text{Fe}/\text{H}], \quad (2)$$

where Δ is the non-LTE abundance correction, which was evaluated from W_{λ} , T_{eff} , $\log g$, and ξ based on the procedure described in §3.3 [i.e., application of Equation (1)] for the case of O I 7771/7774/7775 lines, and $\Delta = 0$ was adopted for the [O I] 6300/6363 lines (cf. §4.2). Note that the solar oxygen abundance was assumed to be 8.93 (in the usual scale of $\log \epsilon_{\text{H}} = 12$) according to Anders & Grevesse (1989). We treat $[\text{O}/\text{Fe}]$ derived from O I 7771–5 lines and [O I] 6300/6363 lines separately, which we hereinafter referred to as $[\text{O}/\text{Fe}]_{77}$ and $[\text{O}/\text{Fe}]_{63}$, respectively. In case that equivalent-width data are available for two or three O I triplet lines, or for both [O I] lines, we calculated $[\text{O}/\text{Fe}]$ for each line and adopted their simple mean to obtain $[\text{O}/\text{Fe}]_{77}$ or $[\text{O}/\text{Fe}]_{63}$.

4.3.2. Results of $[\text{O}/\text{Fe}]$

We tried to use as many W_{λ} data as possible taken from various sources, though our literature survey is not complete. Consequently, ~ 300 stars (~ 200 for $[\text{O}/\text{Fe}]_{77}$ and ~ 100 for $[\text{O}/\text{Fe}]_{63}$) covering a metallicity range of $-3 \lesssim [\text{Fe}/\text{H}] \lesssim 0$ could be analyzed, which are sufficient for statistically meaningful discussion. The resulting $[\text{O}/\text{Fe}]$ ratios (i.e., $[\text{O}/\text{Fe}]_{77}$ or $[\text{O}/\text{Fe}]_{63}$) plotted with respect to $[\text{Fe}/\text{H}]$ for each star are shown in Figure 7a, and the corresponding non-LTE corrections applied to the O I 7771–5 lines are also plotted in Figure 7b. The mean $\langle [\text{O}/\text{Fe}]_{77} \rangle$ and $\langle [\text{O}/\text{Fe}]_{63} \rangle$, averaged in each $[\text{Fe}/\text{H}]$ bin of 0.5 dex, are given in Table 6. The spline-fit curves for the runs of $\langle [\text{O}/\text{Fe}]_{77} \rangle$ and $\langle [\text{O}/\text{Fe}]_{63} \rangle$ with $[\text{Fe}/\text{H}]$ are also depicted in Figure 7a. Our conclusions read from Figure 7 and Table 6 are as follows.

(1) For mildly metal-deficient disk stars ($-1 \lesssim [\text{Fe}/\text{H}] \lesssim 0$), our $[\text{O}/\text{Fe}]_{77}$ and $[\text{O}/\text{Fe}]_{63}$ show a quite similar behavior; i.e., a gradual increase from $[\text{O}/\text{Fe}] \sim 0$ ($[\text{Fe}/\text{H}] \sim 0$) to $[\text{O}/\text{Fe}] \sim +0.5$ ($[\text{Fe}/\text{H}] \sim -1$). This means that our non-LTE corrections are successful to achieve an agreement between the oxygen abundances derived from [O I] 6300/6363 and O I 7771–5 for those population I stars, which is consistent with the conclusion of Takeda et al. (1998).

(2) However, a discrepancy begins to appear when we go toward a lower metallicity further down from $[\text{Fe}/\text{H}] \sim -1$. That is, $[\text{O}/\text{Fe}]_{77}$ still increases with a slight change (i.e., gentler) of the slope from $[\text{O}/\text{Fe}] \sim +0.5$ ($[\text{Fe}/\text{H}] \sim -1$) to $[\text{O}/\text{Fe}] \sim +1$ ($[\text{Fe}/\text{H}] \sim -3$), while $[\text{O}/\text{Fe}]_{63}$ maintains nearly the same value at $[\text{O}/\text{Fe}] \sim +0.5$ on the average over the metallicity range of $-2.5 \lesssim [\text{Fe}/\text{H}] \lesssim -1$ showing a flat plateau. This kind of $[\text{O}/\text{Fe}]_{77}$ vs. $[\text{O}/\text{Fe}]_{63}$ discordance for those conspicuously metal-poor halo stars is just what has been occasionally reported so far (cf. §1). Our analysis thus suggests that this discrepancy in halo stars (amounting to ~ 0.2 – 0.3 dex at $-2.5 \lesssim [\text{Fe}/\text{H}] \lesssim -1.5$)

does exist, without being successfully removed by our non-LTE corrections, unlike the conclusion of Carretta et al. (2000). We will discuss this problem more in detail in the next section.

4.4. O I vs. [O I]: Toward a Unified Solution

4.4.1. Discordance in Halo stars

We have thus confirmed the existence of discrepancy between $[\text{O}/\text{Fe}]_{77}$ and $[\text{O}/\text{Fe}]_{63}$ in the quite metal-poor regime ($-3 \lesssim [\text{Fe}/\text{H}] \lesssim -1$), while a good agreement was obtained in disk stars ($-1 \lesssim [\text{Fe}/\text{H}] \lesssim 0$).

This can not be successfully removed by the non-LTE effect though they surely act in the direction of mitigating the discordance. According to our opinion (cf. §4.1.3), the O I vs. [O I] consistency obtained by Carretta et al. (2000) may be nothing but a fortuitous coincidence caused by their questionable non-LTE corrections for the O I 7771–5 triplet (i.e., systematically overcorrected toward a lower metallicity).

It is also unlikely that systematic errors in the T_{eff} scale (affecting mainly on O I) is responsible for the cause of this discrepancy as has been occasionally suspected (e.g., King 1993), since our analysis in §4.3 is based on the mixed data of equivalent width and atmospheric parameters taken from a variety of sources.

Hence, we would consider that this discordance in halo stars is more or less inevitable as far as the conventional abundance determination method is concerned (i.e., “standard” non-LTE calculations as well as model atmospheres); that is, a challengingly novel modeling would be required to bring them into agreement.

4.4.2. Which Represents the Truth?

Then, which solution is correct, or in other words, which yields the wrong abundances, O I 7771–5 or [O I] 6300/6363 ?

We decided to invoke the following guiding principle: If we assume that the origin of the error is concerned with some stellar physical property which is not appropriately modeled, it is reasonable to expect that abundance discrepancies shown by the erroneous side (whichever O I or [O I]) may show some kind of systematic tendency in terms of stellar parameters (say, T_{eff} or $\log g$), since any stellar physical environment must undergo a distinct change if these parameters vary substantially. And, in an ideal case, the discordance might asymptotically disappear if we go to either limit of the parameter variation.

Motivated by this thought, we paid attention to $[\text{O}/\text{Fe}]_{77} - \langle [\text{O}/\text{Fe}]_{63} \rangle$ (the discrepancy of *each star's* $[\text{O}/\text{Fe}]_{77}$ relative to the *mean* $\langle [\text{O}/\text{Fe}]_{63} \rangle$) and $[\text{O}/\text{Fe}]_{63} - \langle [\text{O}/\text{Fe}]_{77} \rangle$ (the inverse of the above)

within two metallicity bins of $-2.75 \leq [\text{Fe}/\text{H}] < -2.25$ and $-2.25 \leq [\text{Fe}/\text{H}] < -1.75$, where a clear discordance of $\langle [\text{O}/\text{Fe}]_{77} \rangle - \langle [\text{O}/\text{Fe}]_{63} \rangle \sim 0.3$ dex is observed (cf. Table 6). Namely, in the former case, on the assumption that O I abundances are “wrong”, we investigate their departure from the “correct” [O I] abundance; while in the latter case, we consider just the opposite. The dependence of former quantity for each stars is plotted in Figure 8 with respect to T_{eff} (a) and $\log g$ (b), while that of the latter is similarly shown in Figure 9.

In Figure 8, what we observe is only a large scatter around the mean of $\sim +0.3$, which is presumably caused by the strong T_{eff} -sensitivity of these high-excitation O I 7771–5 lines.

Interestingly, however, we notice a weak trend in Figure 9, i.e., $|[\text{O}/\text{Fe}]_{63} - \langle [\text{O}/\text{Fe}]_{77} \rangle|$ (the extent of the discrepancy shown by the [O I] abundance) appears to decrease with an increase in T_{eff} as well as in $\log g$ and approaches zero toward the high- T_{eff} /high- $\log g$ limit, which is more clearly observable if we confine ourselves to only the data in the $-2.75 \leq [\text{Fe}/\text{H}] < -2.25$ bin (open triangles). If this tendency is real, it may be reasonable to speculate that systematic errors are involved in our [O I] abundances.

4.4.3. Possibility of [O I] Weakening

Let us assume as a working hypothesis that [O I] lines yield abundances that are erroneously weak, and the extent of the error increases with a lowering of T_{eff} as well as in $\log g$, What could cause this effect?

Since the possibility of a non-LTE effect may be ruled out for these [O I] lines as described in §4.2, an interpretation which appears promising to us is the hypothesis once proposed by Langer (1991); that is, a weakening mechanism invoking that the [O I] emission coming from a circumstellar envelope overlaps the photospheric [O I] absorption line (see also Takeda et al. 2000). We suspect that the essence of this weak trend implied by Figures 9a and b, an increase of the discrepancy with a lowering of T_{eff} as well as $\log g$, is nothing but its $\log g$ -dependence, since T_{eff} and $\log g$ show a close positive correlation in metal-poor giants reflecting their positions on the HR diagram (see, e.g., Fig. 3 of Pilachowski et al. 1996). According to this view, the implication of Figure 9 is that a weakening of [O I] 6300/6363 lines becomes more conspicuous as the surface gravity is lowered (i.e., more extended atmosphere). It is then natural to imagine that a circumstellar emission (if any exists) may have something to do with such an [O I] weakening.

Then, why the O I vs. [O I] discrepancy is observed only in considerably metal-poor halo stars, while not in moderately metal-deficient disk stars? It may be attributed to the intrinsic weakness of the [O I] absorption, for which even a slight contribution of extra emission would cause an appreciable affection to the line strength in the relative sense. Or alternatively, a selection effect may partly be responsible for this; namely, observations of [O I] lines in very metal-poor stars are almost exclusively restricted to low-gravity giants because they are too weak to be measured in dwarfs owing to the conspicuous luminosity effect, while observations of [O I] lines are available

for dwarfs as well as for giants in the case of disk stars.

Admittedly, what has been described above is not so much strictly logical as rather imaginative. We suggest that the decisive touchstone would be a trial of extremely high S/N ($\sim 10^3$) observations of [O I] lines in very metal poor stars (giants as well as high-gravity dwarfs). If the “filled-in emission” hypothesis is really the case, some characteristic signature of overlapping component is expected in the line profile of [O I] absorption lines in giants. And if our interpretation is correct, the [O I] vs. O I discrepancy would not be observed any more in very metal-poor *dwarfs* (such like HD 140283 in Figure 9).

5. CONCLUSION

For the purpose of investigating the line formation of O I 7771–5 lines of IR triplet and [O I] 6300/6363 lines especially concerning the consistency of the oxygen abundances derived from these two in metal-poor disk/halo stars, we carried out non-LTE calculations with a new atomic model of oxygen on an extensive grid of model atmospheres ($4500 \text{ K} \leq T_{\text{eff}} \leq 6500 \text{ K}$, $1 \leq \log g \leq 5$, and $-3 \leq [\text{Fe}/\text{H}] \leq 0$).

In order to make the resulting non-LTE abundance corrections of O I 7771–5 lines more useful for practical applications, we derived an analytical formula with appropriate coefficients computed and tabulated in a grid of atmospheric parameters, by which the non-LTE correction is easily evaluated for any given set of W_λ , T_{eff} , $\log g$ and ξ .

We discussed our non-LTE corrections for the O I triplet lines while comparing them with those derived from other studies published so far. The most important result of this comparison is that we could not reproduce the trend of the non-LTE correction deived by Carretta et al. (2000), the systematic [Fe/H]-dependence of which is essentially the reason for their success of accomplishing the O I vs. [O I] consistency. We consider that their consequence should be viewed with caution, until the cause of such a metallicity effect is reasonably clarified.

Based on our calculations, we arrived at a robust conclusion that the non-LTE effect for the [O I] 6300/6363 lines can be safely negligible and thus LTE is a valid approximation.

We reanalyzed the various published equivalent-width data of O I 7771–5 and [O I] 6300/6363 lines (while the non-LTE effect is taken into account for the former based on our calculations), in order to study the behavior of [O/Fe] vs. [Fe/H] relation over a wide range of metallicity ($-3 \lesssim [\text{Fe}/\text{H}] \lesssim 0$). While [O/Fe]₇₇ and [O/Fe]₆₃ were found to agree with each other for disk stars ($-1 \lesssim [\text{Fe}/\text{H}] \lesssim 0$), the existence of a systematic discrepancy was confirmed for halo stars ($-3 \lesssim [\text{Fe}/\text{H}] \lesssim -1$) amounting to [O/Fe]₇₇ – [O/Fe]₆₃ ~ 0.3 dex at $-3 \lesssim [\text{Fe}/\text{H}] \lesssim -2$.

Inspecting the dependence of discrepancy upon T_{eff} and $\log g$, we suspect that the cause of the discordance (increasing with a lowered $\log g$) is on the side of the [O I] lines, which may have been somehow weakened by a mechanism which is not taken into account in the standard line formation

calculation. Langer’s (1991) hypothesis (an overlapping emission from the extended atmosphere) may be worth further investigation as a possibility for such a line-weakening mechanism.

If our view, that O I lines may be more reliable than [O I] lines, is correct, it naturally lends support for the “rising” tendency ($[O/Fe]_{77}$) rather than the “flat” trend ($[O/Fe]_{63}$) as the [O/Fe] ratio behavior of metal-poor halo stars; i.e., from $[O/Fe] \sim +0.5$ ($[Fe/H] \sim -1$) to $[O/Fe] \sim +1$ ($[Fe/H] \sim -3$), which is in agreement with the recent OH results (e.g., Boesgaard et al. 1999; Israelian et al. 1998, 2001).

A. ON THE EFFECT AND TREATMENT OF H I COLLISION

The collisional rate due to neutral hydrogen atoms is regarded to be one of the important ambiguous factors in non-LTE calculations on late-type stellar atmospheres. A rough classical formula derived by Steenbock and Holweger (1984) is available for this (see Takeda 1991 for more detailed description on the standard classical recipe adopted). However, because of its nature of only an order-of-magnitude accuracy, a correction factor is often introduced, by which this classical rate is to be multiplied. We express this factor as 10^h by using the logarithmic correction (h). Negative h leads to the suppression of the H I collisional rates compared to the classical case, which increases the extent of the NLTE abundance correction ($|\Delta \log \epsilon|$); and vice versa. This situation is depicted in Figure 10, where the h -dependence of $\Delta \log \epsilon$ for the O I 7774.18 line is shown, which was calculated for selected representative models.

As mentioned in §2.1, we used $h = 0$ (as was done by Takeda 1991, 1994) throughout this paper, which means the simple adoption of the classical treatment without any correction. This choice stems from the detailed investigation of Takeda (1995), where $h = 0.0(\pm 0.5)$ was concluded from the analysis of the solar flux spectrum based on (1) the comparison of the solar oxygen abundance derived from O I 7771–5 lines with the average of other 15 weaker lines and (2) the profile-fitting of these near-IR triplet lines.

It may be worthwhile, from another point of view, to check the consistency of this treatment on nearby solar-type stars, which have been recently analyzed by Takeda et al. (2001) to study the abundance characteristics of planet-harboring stars.

Figure 11 shows the comparison of the non-LTE abundance of O I 7771–5 triplet (with the NLTE correction obtained by using the formula described in this study) with the LTE abundance of O I 6158.2 (a) and [O I] 6300.3 (b), which were derived from either equivalent-widths or spectrum-synthesis technique (with the same line data as given in table 2) as described in Takeda et al. (2001). Note that we neglected the non-LTE corrections for these latter two lines since their extents are $\lesssim 0.05$ dex at most for those solar-type dwarf stars (cf. Tables 3 and 8).

We can see from Figure 11(a) that $\log \epsilon_{6158}^O$ and $\log \epsilon_{7771-5}^O$ are in satisfactory agreement with each other, which confirms that our choice of $h = 0$ is surely reasonable.

Meanwhile, for the case of 6300 vs. 7771–5 comparison shown in Figure 11(b), the scatter is comparatively large, which makes this figure less useful for the purpose of checking the adequacy of h . Presumably, this appreciable spread may be due to the large difference in the T_{eff} -sensitivity of these two lines (in contrast to the case of 7771–5 and 6158 which have almost the same T_{eff} -dependence). A close inspection of Figure 11(b) suggests that the 6300 abundance tends to be somewhat larger especially for the case of higher oxygen abundance ($\log \epsilon \gtrsim 0.0$), for which two reasons may be suspected; i.e., the possible inaccuracy in the adopted gf value and/or the effect of blending. That is, according to the recent study of the solar [O I] 6300 line profile by Allende Prieto et al. (2001), the Ni I line at 6300.34 Å makes an appreciable contribution to this feature. Our neglect of this effect may have cause an overestimation. In addition, their paper suggests that the most recently calculated gf value is $\log gf([\text{O I}] 6300) = -9.72$, which is by +0.1 dex larger than that adopted in this study. This may have resulted in an overestimated $\log \epsilon_{6300}^{\text{O}}$.

We finally remark that, even if our $\log \epsilon_{6300}^{\text{O}}$ values have been overestimated either due to the use of underestimated $\log gf$ or due to the blending effect of the Ni line, our conclusion of 6300 vs. 7771–5 abundance discrepancy (cf. §4.3.2) can not be changed at all (i.e., because the discordance would become even larger).

B. INTERPRETATION OF THE TRIPLET-LINE FORMATION WITH THE TWO-LEVEL-ATOM MODEL

The results found in §3.3, that the NLTE correction for the O I 7773 triplet (for given T_{eff} , $\log g$, and ξ) is a monotonic function of W_{λ} irrespective of the metallicity, might at first appear strange. However, a reasonable explanation can be made for this tendency as described below (see also §2.2 of Takeda 1994).

The key to understanding this is the fact that the non-LTE departure of this triplet is (1) essentially due to the dilution of the line source function (S_{L}), which is caused by an appreciable underpopulation of the upper term (3p ^5P) by the escape of photons from the surface at the optically-thin region, and (2) *not* due to the variation of the line-opacity since the lower term (3s $^5\text{S}^{\circ}$) of this transition is nearly in LTE³ in the line-forming region of solar-type stars (cf. Figure 7 in Takeda 1994). In such a case, the formation of this O I triplet can be interpreted by the classical scattering model with the simple “two-level plus continuum” atom extensively discussed by Hummer (1968). Even with this simple model, he could show that the extent of the dilution in S_{L} is determined by (a) the photon-destruction probability defined as the ratio of the radiative to collisional (downward) transition probability ($\epsilon' \simeq C_{21}/A_{21}$; cf. equation [11-7] in Mihalas 1978) and (b) the relative importance of the thermalizing continuum determined by the continuum-to-line

³This is attributed to the interaction with the ground term (i.e., the direct collisional coupling and/or via the collision with the closely lying 3s $^3\text{S}^{\circ}$ term connecting to the ground term by thermalizing radiation) where most of the oxygen atoms are populated in LTE.

opacity ratio $\beta \equiv \kappa_C/\kappa_L$ (cf. Hummer 1968). Namely, the problem in question can be explained as follows:

- (i) For the same ϵ' (i.e., atmospheres with the same temperature and density), the extent of β essentially controls the dilution of S_L is (i.e. the smaller β , the more enhanced NLTE effect).
- (ii) On the other hand, the extent of the dilution in S_L naturally determines the importance of the NLTE effect (i.e., the extent of the NLTE correction) as well as the strength of the observed line (i.e., equivalent width) in this case of scattering line formation.

We now understand from “fact (ii)” that a close relationship exists between the strength of the O I 7771–5 triplet lines and the corresponding non-LTE corrections. Meanwhile, “fact (i)” simply tells that the essential key parameter is β only (for the same ϵ'), which further suggests that the difference in the metallicity does not play any essential role in the present problem. Namely, as far as the continuum-to-line opacity ratio is the same (along with T_{eff} and $\log g$), the same extent of S_L , the same equivalent width, and the same non-LTE correction are expected irrespective of the metallicity, thus yielding the same W_λ vs. $\log \epsilon$ correlation.

It may be instructive to compare the results from a simple simulation based on such a “two-level plus continuum” model with the actually obtained W_λ vs. $\log \epsilon$ relation shown in Figure 1. Though the value of ϵ' is strongly depth-dependent in real atmospheres, we found $\epsilon' \sim 1$ (dwarfs) and $\epsilon' \sim 0.1$ (supergiants) in the line-forming region from actual model calculations. We adopted the Milne–Eddington model assuming the depth-independent line-to-continuum opacity ratio η ($\equiv 1/\beta$) and the linear form of the Planck function, $B(\tau) \equiv B_0 + B_1\tau = B_0(+B_1/B_0\tau)$ (τ : continuum optical depth). We fixed $B_0 = 1$ and changed the gradient $B_1 (= B_1/B_0)$. Again the determination of this gradient at 7773 Å is rather difficult since it is not linear in terms of τ in actual cases, but we tentatively chose by inspection of the model atmospheres $B_1 = 2$ (low T_{eff} case) and $B_1 = 1$ (high T_{eff} case). Hence, the radiative transfer problems (two-level-atom plus continuum, complete frequency redistribution, and the pure Gaussian line profile) investigated by Hummer (1968) were numerically solved by using the Rybicki’s (1971) scheme for various values of η ($\equiv 1/\beta$) ranging from 10^{-2} to 10^3 for each of the three combinations of (B_1, ϵ') ; (2, 1), (2, 0.1), and (1, 1). And then the emergent flux spectra were computed from the resulting solution of the source function (NLTE case), along with the LTE case of $S_L = B$ (i.e., the limit of $\epsilon' \rightarrow \infty$), to obtain the equivalent width (W).

In Figure 12 are shown the LTE and NLTE curves of growth [panel (a)], and the corresponding NLTE correction $\Delta \log \eta$ ($\equiv \log \eta_{\text{NLTE}} - \log \eta_{\text{LTE}}$; i.e., difference of the abscissa for a given W) as a function of W_{NLTE} [panel (b)]. We can see from Figure 12(b) that the computed $\Delta \log \eta$ vs. W_{NLTE} curves well resemble (at least qualitatively) the W_λ vs. $\log \epsilon$ relations observed in Figure 1, in the sense that they can be approximated with the functional form of Eq. (1).

It is worthwhile commenting on the effects of changing ϵ' or B_1 observed in Figure 12(b). As expected, the extent of the NLTE correction increases with a decrease in ϵ' . Meanwhile, that $|\Delta \log \eta|$ is larger for a smaller gradient (B_1) of the Planck function may be attributed to the decreased sensitivity of W_{LTE} (to a change in η) owing to the lessened gradient (i.e., W_{LTE} is

relatively more affected by the Planck function B , in contrast to the NLTE case which is mainly controlled by the radiation field). It should be noted that these two qualitative behaviors concluded from our simple model reasonably explain the tendencies observed in Figure 1. That is, the larger $|\Delta\epsilon|$ for a lowered gravity (at a given W_λ) is reasonably explained by the ϵ' -dependence described above. Meanwhile, regarding the tendency of larger $|\Delta\epsilon|$ for a higher T_{eff} (at a given W_λ), the above-mentioned effect of decreased B_1 may be responsible for it.

REFERENCES

- Abia, C., & Rebolo, R. 1989, *ApJ*, 347, 186
- Allende Prieto, C., Lambert, D. L., & Asplund, M. 2001, *ApJ*, 556, L63
- Anders, E., & Grevesse, N. 1989, *Geochim. Cosmochim. Acta*, 53, 197
- Auer, L. H., & Mihalas, D. 1973, *ApJ*, 184, 151
- Barbuy, B. 1988, *A&A*, 191, 121
- Barbuy, B., & Erdelyi-Mendes, M. 1989, *A&A*, 214, 239
- Boesgaard, A. M., & King, J. R. 1993, *AJ*, 106, 2309
- Boesgaard, A. M., King, J. R., Deliyannis, C. P., & Vogt, S. S. 1999, *AJ*, 117, 492
- Carretta, E., Gratton, R. G., & Sneden, C. 2000, *A&A*, 356, 238
- Cavallo, R. M., Pilachowski, C. A., & Rebolo, R. 1997, *PASP*, 109, 226
- Edvardsson, B., Andersen, J., Gustafsson, B., Lambert, D. L., Nissen, P. E., & Tomkin, J. 1993, *A&A*, 275, 101
- Gratton, R. G., Carretta, E., Eriksson, K., & Gustafsson, B. 1999, *A&A*, 350, 955
- Holweger, H., & Müller, E. A. 1974, *Solar Phys.*, 39, 19
- Hummer, D. G. 1968, *MNRAS*, 138, 73
- Israelian, G., García López, R. J., & Rebolo, R. 1998, *ApJ*, 507, 805
- Israelian, G., Rebolo, R., García López, R. J., Bonifacio, P., Molaro, P., Basri, G., & Shchukina, N. 2001, *astro-ph/0101032*
- King, J. R. 1993, *AJ*, 106, 1206
- King, J. R. 1994, *ApJ*, 436, 331
- King, J. R. 2000, *AJ*, 120, 1056
- Kiselman, D. 1991, *A&A*, 245, L9
- Kraft, R. P., Sneden, C., Langer, G. E., & Prosser, C. F. 1992, *AJ*, 104, 645
- Kupka, F., Piskunov, N. E., Ryabchikova, T. A., Stempels, H. C., & Weiss, W. W. 1999, *A&AS*, 138, 119
- Kurucz, R. L. 1993, Kurucz CD-ROM No.13 (Harvard-Smithsonian Center for Astrophysics)

- Kurucz, R. L., & Bell, B. 1995, Kurucz CD-ROM No.23 (Harvard-Smithsonian Center for Astrophysics)
- Kurucz, R. L., & Peytremann, E. 1972, Smithsonian Astrophys. Spec. Rept., No. 362
- Langer, G. E., 1991, PASP, 103, 177
- Leushin, V. V., & Topil'skaya, G. P. 1987, Astrophysics, 25, 415
- Mihalas, D. 1978, Stellar Atmospheres, 2nd ed. (San Francisco: W. H. Freeman and Company)
- Mishenina, T. V., Korotin, S. A., Klochkova, V. G., & Panchuk, V. E. 2000, A&A, 353, 978
- Morton, D. C. 1991, ApJS, 77, 119
- Osterbrock, D. E. 1974, Astrophysics of Gaseous Nebulae (San Francisco: W. H. Freeman and Company), p. 244
- Pilachowski, C. A., Sneden, C., & Kraft, R. P. 1996, AJ, 111, 1689
- Rybicki, G. 1971, J. Quant. Spect. Rad. Trans., 11, 589
- Sneden, C., Kraft, R. P., Prosser, C. F., & Langer, G. E. 1991, AJ, 102, 2001
- Sneden, C., Lambert, D., & Whitaker, R. W. 1979, ApJ, 234, 964
- Steenbock, W., & Holweger, H. 1984, A&A, 130, 319
- Takeda, Y. 1991, A&A, 242, 455
- Takeda, Y. 1992, PASJ, 44, 309
- Takeda, Y. 1994, PASJ, 46, 53
- Takeda, Y. 1995, PASJ, 47, 463
- Takeda, Y., Kawanomoto, S., & Sadakane, K. 1998, PASJ, 50, 97
- Takeda, Y., Takada-Hidai, M., Sato, S., Sargent, W. L. W., Lu, L., Barlow, T. A., & Jugaku, J. 2000, ApJ, submitted (astro-ph/0007007)
- Takeda, Y., Sato, B., Kambe, E., Aoki, W., Honda, S., Kawanomoto, S., Masuda, S., Izumiura, H., Watanabe, E., Koyano, H., Maehara, H., Norimoto, Y., Okada, T., Shimizu, Y., Uruguchi, F., Yanagisawa, K., Yoshida, M., Miyama, S., & Ando, H. 2001, PASJ, 53, 1211
- Tomkin, J., Lemke, M., Lambert, D. L., & Sneden, C. 1992, AJ, 104, 1568
- van Regemorter, H. 1962, ApJ, 136, 906

Table 1: Data of Neutral Oxygen Lines Adopted for Abundance Calculations.

RMT	λ (Å)	χ (eV)	$\log gf$	Gammar	Gammas	Gammaw
1	7771.944	9.146	0.324	7.52	-5.55	-7.65*
1	7774.166	9.146	0.174	7.52	-5.55	-7.65*
1	7775.388	9.146	-0.046	7.52	-5.55	-7.65*
...	6300.304	0.000	-9.819	-2.17	-7.83*	-8.13*
...	6363.776	0.020	-10.303	-2.17	-7.83*	-8.13*
10	6158.149	10.741	-1.891	7.62	-3.96	-7.23*
10	6158.172	10.741	-1.031	7.62	-3.96	-7.23*
10	6158.187	10.741	-0.441	7.62	-3.96	-7.23*

NOTE — All data are were taken from Kurucz & Bell’s (1995) compilation as far as available.
 Followed by first four self-explanatory columns, damping parameters are given in the last three columns:
 Gammar is the radiation damping constant, $\log \gamma_{\text{rad}}$.
 Gammae is the Stark damping width per electron density at 10^4 K, $\log(\gamma_e/N_e)$.
 Gammaw is the van der Waals damping width per hydrogen density at 10^4 K, $\log(\gamma_w/N_H)$.
 * Computed as default values in the Kurucz’s WIDTH program (cf. Leusin, Topil’skaya 1987).

Table 2: NLTE abundance correction for O I 7774.17 ($\xi = 2 \text{ km s}^{-1}$).

Code	A_1^a (W_1^{LTE})	W_1^{NLTE}	A_1^N	A_1^L	Δ_1	A_2^a (W_2^{LTE})	W_2^{NLTE}	A_2^N	A_2^L	Δ_2	A_3^a (W_3^{LTE})	W_3^{NLTE}	A_3^N	A_3^L	Δ_3
t65g50m0	8.630 (75.86)	83.18	8.626	8.723	-0.097	8.930 (100.00)	112.20	8.921	9.051	-0.130	9.230 (128.82)	147.91	9.225	9.390	-0.165
t65g40m0	8.630 (95.50)	117.49	8.636	8.911	-0.275	8.930 (120.23)	151.36	8.942	9.310	-0.368	9.230 (144.54)	186.21	9.234	9.661	-0.427
t65g30m0	8.630 (117.49)	158.49	8.616	9.189	-0.573	8.930 (138.04)	194.98	8.926	9.629	-0.703	9.230 (162.18)	229.09	9.216	9.973	-0.757
t65g20m0	8.630 (138.04)	208.93	8.641	9.564	-0.923	8.930 (158.49)	245.47	8.953	9.954	-1.001	9.230 (181.97)	275.42	9.220	10.209	-0.989
t65g10m0	8.630 (154.88)	251.19	8.647	9.899	-1.252	8.930 (173.78)	281.84	8.925	10.187	-1.262	9.230 (194.98)	316.23	9.251	10.442	-1.191
t60g50m0	8.630 (51.29)	53.70	8.630	8.684	-0.054	8.930 (70.79)	75.86	8.928	9.001	-0.073	9.230 (95.50)	104.71	9.240	9.334	-0.094
t60g40m0	8.630 (69.18)	81.28	8.639	8.805	-0.166	8.930 (91.20)	107.15	8.924	9.149	-0.225	9.230 (114.82)	138.04	9.226	9.508	-0.282
t60g30m0	8.630 (91.20)	117.49	8.623	8.993	-0.370	8.930 (112.20)	151.36	8.940	9.439	-0.499	9.230 (134.90)	181.97	9.216	9.798	-0.582
t60g20m0	8.630 (114.82)	162.18	8.620	9.296	-0.676	8.930 (134.90)	199.53	8.946	9.783	-0.837	9.230 (158.49)	229.09	9.214	10.111	-0.897
t60g10m0	8.630 (138.04)	208.93	8.611	9.613	-1.002	8.930 (158.49)	245.47	8.937	10.036	-1.099	9.230 (181.97)	275.42	9.218	10.315	-1.097
t55g50m0	8.630 (26.92)	28.18	8.630	8.657	-0.027	8.930 (40.74)	41.69	8.923	8.958	-0.035	9.230 (56.23)	60.26	9.240	9.286	-0.046
t55g40m0	8.630 (41.69)	45.71	8.628	8.715	-0.087	8.930 (56.23)	63.10	8.921	9.042	-0.121	9.230 (74.13)	85.11	9.225	9.381	-0.156
t55g30m0	8.630 (60.26)	72.44	8.627	8.840	-0.213	8.930 (77.62)	97.72	8.941	9.233	-0.292	9.230 (97.72)	123.03	9.223	9.585	-0.362
t55g20m0	8.630 (83.18)	109.65	8.622	9.024	-0.402	8.930 (102.33)	141.25	8.942	9.477	-0.535	9.230 (123.03)	169.82	9.222	9.857	-0.635
t55g10m0	8.630 (109.65)	154.88	8.623	9.310	-0.687	8.930 (128.82)	186.21	8.912	9.746	-0.834	9.230 (147.91)	218.78	9.222	10.149	-0.927
t50g50m0	8.630 (10.72)	10.96	8.634	8.646	-0.012	8.930 (16.98)	17.38	8.936	8.950	-0.014	9.230 (25.70)	26.30	9.236	9.254	-0.018
t50g40m0	8.630 (18.62)	19.50	8.623	8.665	-0.042	8.930 (26.92)	28.84	8.928	8.982	-0.054	9.230 (38.02)	40.74	9.228	9.297	-0.069
t50g30m0	8.630 (30.90)	34.67	8.630	8.736	-0.106	8.930 (42.66)	47.86	8.920	9.066	-0.146	9.230 (54.95)	64.57	9.234	9.417	-0.183
t50g20m0	8.630 (47.86)	57.54	8.629	8.843	-0.214	8.930 (61.66)	75.86	8.917	9.196	-0.279	9.230 (77.62)	97.72	9.224	9.570	-0.346
t50g10m0	8.630 (70.79)	91.20	8.630	8.985	-0.355	8.930 (87.10)	117.49	8.945	9.411	-0.466	9.230 (107.15)	141.25	9.218	9.768	-0.550
t45g50m0	8.630 (2.19)	2.19	8.628	8.633	-0.005	8.930 (3.80)	3.80	8.929	8.935	-0.006	9.230 (6.31)	6.31	9.225	9.232	-0.007
t45g40m0	8.630 (5.25)	5.37	8.627	8.644	-0.017	8.930 (8.32)	8.51	8.930	8.950	-0.020	9.230 (12.59)	12.88	9.227	9.251	-0.024
t45g30m0	8.630 (10.47)	11.22	8.639	8.684	-0.045	8.930 (15.14)	16.22	8.923	8.979	-0.056	9.230 (21.38)	23.44	9.239	9.309	-0.070
t45g20m0	8.630 (19.05)	20.89	8.623	8.712	-0.089	8.930 (26.30)	29.51	8.927	9.042	-0.115	9.230 (35.48)	39.81	9.224	9.364	-0.140
t45g10m0	8.630 (32.36)	38.02	8.634	8.795	-0.161	8.930 (42.66)	50.12	8.921	9.125	-0.204	9.230 (54.95)	66.07	9.244	9.496	-0.252
t65g50m1	8.130 (38.02)	42.66	8.137	8.204	-0.067	8.430 (57.54)	63.10	8.424	8.511	-0.087	8.730 (81.28)	91.20	8.735	8.855	-0.120
t65g40m1	8.130 (56.23)	69.18	8.132	8.323	-0.191	8.430 (77.62)	97.72	8.438	8.712	-0.274	8.730 (100.00)	128.82	8.737	9.113	-0.376
t65g30m1	8.130 (77.62)	107.15	8.125	8.562	-0.437	8.430 (97.72)	141.25	8.430	9.054	-0.624	8.730 (117.49)	173.78	8.717	9.497	-0.780
t65g20m1	8.130 (100.00)	154.88	8.124	8.980	-0.856	8.430 (120.23)	190.55	8.426	9.485	-1.059	8.730 (138.04)	223.87	8.721	9.881	-1.160
t65g10m1	8.130 (114.82)	199.53	8.132	9.413	-1.281	8.430 (134.90)	234.42	8.432	9.852	-1.420	8.730 (154.88)	269.15	8.755	10.196	-1.441
t60g50m1	8.130 (22.91)	24.55	8.135	8.173	-0.038	8.430 (37.15)	39.81	8.437	8.483	-0.046	8.730 (56.23)	60.26	8.737	8.795	-0.058
t60g40m1	8.130 (36.31)	42.66	8.134	8.243	-0.109	8.430 (53.70)	63.10	8.428	8.572	-0.144	8.730 (74.13)	89.13	8.733	8.926	-0.193
t60g30m1	8.130 (54.95)	70.79	8.126	8.375	-0.249	8.430 (74.13)	100.00	8.440	8.789	-0.349	8.730 (95.50)	128.82	8.722	9.191	-0.469
t60g20m1	8.130 (75.86)	109.65	8.120	8.615	-0.495	8.430 (97.72)	144.54	8.438	9.134	-0.696	8.730 (117.49)	177.83	8.739	9.613	-0.874
t60g10m1	8.130 (100.00)	158.49	8.138	9.036	-0.898	8.430 (120.23)	190.55	8.418	9.511	-1.093	8.730 (138.04)	223.87	8.724	9.939	-1.215
t55g50m1	8.130 (11.22)	11.75	8.131	8.151	-0.020	8.430 (19.50)	20.42	8.435	8.458	-0.023	8.730 (31.62)	33.11	8.732	8.759	-0.027
t55g40m1	8.130 (19.95)	21.88	8.131	8.192	-0.061	8.430 (30.90)	34.67	8.429	8.504	-0.075	8.730 (46.77)	52.48	8.735	8.833	-0.098
t55g30m1	8.130 (32.36)	39.81	8.138	8.284	-0.146	8.430 (47.86)	58.88	8.436	8.622	-0.186	8.730 (66.07)	81.28	8.722	8.957	-0.235
t55g20m1	8.130 (51.29)	67.61	8.126	8.410	-0.284	8.430 (69.18)	93.33	8.421	8.790	-0.369	8.730 (89.13)	123.03	8.730	9.221	-0.491
t55g10m1	8.130 (72.44)	107.15	8.139	8.645	-0.506	8.430 (93.33)	138.04	8.435	9.105	-0.670	8.730 (112.20)	169.82	8.736	9.580	-0.844
t50g50m1	8.130 (4.27)	4.37	8.130	8.140	-0.010	8.430 (7.76)	7.94	8.427	8.438	-0.011	8.730 (13.80)	14.13	8.736	8.748	-0.012
t50g40m1	8.130 (8.51)	8.91	8.129	8.158	-0.029	8.430 (14.13)	15.14	8.433	8.468	-0.035	8.730 (22.39)	23.99	8.729	8.771	-0.042
t50g30m1	8.130 (15.14)	17.38	8.134	8.212	-0.078	8.430 (23.99)	27.54	8.437	8.532	-0.095	8.730 (35.48)	40.74	8.730	8.845	-0.115
t50g20m1	8.130 (26.30)	32.36	8.123	8.282	-0.159	8.430 (38.90)	48.98	8.440	8.636	-0.196	8.730 (53.70)	67.61	8.731	8.968	-0.237
t50g10m1	8.130 (43.65)	57.54	8.133	8.398	-0.265	8.430 (58.88)	79.43	8.427	8.761	-0.334	8.730 (77.62)	104.71	8.730	9.150	-0.420
t45g50m1	8.130 (0.69)	0.69	8.126	8.131	-0.005	8.430 (1.35)	1.35	8.428	8.433	-0.005	8.730 (2.57)	2.57	8.728	8.734	-0.006
t45g40m1	8.130 (2.29)	2.34	8.130	8.144	-0.014	8.430 (4.17)	4.27	8.432	8.447	-0.015	8.730 (7.08)	7.41	8.735	8.752	-0.017
t45g30m1	8.130 (5.13)	5.37	8.124	8.159	-0.035	8.430 (8.51)	9.12	8.430	8.471	-0.041	8.730 (13.49)	14.45	8.733	8.781	-0.048
t45g20m1	8.130 (10.00)	11.22	8.131	8.204	-0.073	8.430 (15.49)	17.78	8.436	8.524	-0.088	8.730 (23.44)	26.30	8.730	8.833	-0.103
t45g10m1	8.130 (18.62)	21.88	8.133	8.251	-0.118	8.430 (27.54)	32.36	8.431	8.575	-0.144	8.730 (38.02)	45.71	8.733	8.907	-0.174

Table 2: (Continued.)

Code	A_1^{a} (W_1^{LTE})	W_1^{NLTE}	A_1^{N}	A_1^{L}	Δ_1	A_2^{a} (W_2^{LTE})	W_2^{NLTE}	A_2^{N}	A_2^{L}	Δ_2	A_3^{a} (W_3^{LTE})	W_3^{NLTE}	A_3^{N}	A_3^{L}	Δ_3
t65g50m2	7.130 (5.75)	6.31 7.129 7.173	-0.044	7.430 (10.72)	11.75 7.433 7.481	-0.048	7.730 (18.62)	20.42 7.725 7.780	-0.055						
t65g40m2	7.130 (11.22)	13.80 7.130 7.236	-0.106	7.430 (19.50)	23.99 7.430 7.554	-0.124	7.730 (31.62)	38.90 7.727 7.875	-0.148						
t65g30m2	7.130 (20.42)	28.84 7.136 7.349	-0.213	7.430 (32.36)	45.71 7.423 7.675	-0.252	7.730 (48.98)	69.18 7.731 8.045	-0.314						
t65g20m2	7.130 (36.31)	53.70 7.123 7.449	-0.326	7.430 (52.48)	79.43 7.421 7.858	-0.437	7.730 (70.79)	109.65 7.727 8.329	-0.602						
t65g10m2	7.130 (50.12)	85.11 7.124 7.687	-0.563	7.430 (69.18)	117.49 7.426 8.198	-0.772	7.730 (87.10)	151.36 7.731 8.757	-1.026						
t60g50m2	7.130 (2.82)	3.02 7.134 7.163	-0.029	7.430 (5.37)	5.75 7.433 7.463	-0.030	7.730 (9.77)	10.47 7.726 7.759	-0.033						
t60g40m2	7.130 (5.75)	6.76 7.133 7.205	-0.072	7.430 (10.47)	12.30 7.432 7.512	-0.080	7.730 (18.20)	21.38 7.733 7.824	-0.091						
t60g30m2	7.130 (11.48)	14.79 7.126 7.269	-0.143	7.430 (19.50)	25.70 7.434 7.602	-0.168	7.730 (30.90)	40.74 7.727 7.924	-0.197						
t60g20m2	7.130 (20.89)	30.90 7.134 7.386	-0.252	7.430 (33.11)	48.98 7.435 7.734	-0.299	7.730 (48.98)	70.79 7.725 8.081	-0.356						
t60g10m2	7.130 (37.15)	54.95 7.131 7.459	-0.328	7.430 (53.70)	79.43 7.422 7.852	-0.430	7.730 (72.44)	109.65 7.737 8.322	-0.585						
t55g50m2	7.130 (1.15)	1.20 7.129 7.146	-0.017	7.430 (2.29)	2.34 7.426 7.444	-0.018	7.730 (4.37)	4.57 7.730 7.749	-0.019						
t55g40m2	7.130 (2.45)	2.75 7.133 7.181	-0.048	7.430 (4.68)	5.25 7.433 7.485	-0.052	7.730 (8.51)	9.55 7.729 7.786	-0.057						
t55g30m2	7.130 (5.25)	6.31 7.125 7.223	-0.098	7.430 (9.33)	11.48 7.428 7.537	-0.109	7.730 (16.22)	19.95 7.730 7.853	-0.123						
t55g20m2	7.130 (10.96)	14.45 7.129 7.288	-0.159	7.430 (18.20)	24.55 7.429 7.615	-0.186	7.730 (28.84)	38.90 7.726 7.946	-0.220						
t55g10m2	7.130 (20.42)	29.51 7.134 7.375	-0.241	7.430 (31.62)	45.71 7.423 7.713	-0.290	7.730 (46.77)	67.61 7.734 8.084	-0.350						
t50g50m2	7.130 (0.38)	0.39 7.134 7.144	-0.010	7.430 (0.74)	0.76 7.426 7.436	-0.010	7.730 (1.48)	1.51 7.730 7.741	-0.011						
t50g40m2	7.130 (0.87)	0.93 7.131 7.157	-0.026	7.430 (1.70)	1.82 7.430 7.457	-0.027	7.730 (3.31)	3.47 7.726 7.754	-0.028						
t50g30m2	7.130 (1.91)	2.19 7.129 7.190	-0.061	7.430 (3.63)	4.17 7.428 7.492	-0.064	7.730 (6.76)	7.76 7.732 7.803	-0.071						
t50g20m2	7.130 (4.17)	5.13 7.127 7.228	-0.101	7.430 (7.76)	9.55 7.432 7.544	-0.112	7.730 (13.18)	16.60 7.730 7.861	-0.131						
t50g10m2	7.130 (9.55)	12.30 7.134 7.272	-0.138	7.430 (16.22)	20.89 7.431 7.591	-0.160	7.730 (25.70)	33.11 7.724 7.914	-0.190						
t45g50m2	7.130 (0.07)	0.07 7.134 7.141	-0.007	7.430 (0.13)	0.13 7.432 7.439	-0.007	7.730 (0.26)	0.27 7.733 7.740	-0.007						
t45g40m2	7.130 (0.22)	0.23 7.132 7.147	-0.015	7.430 (0.44)	0.46 7.433 7.448	-0.015	7.730 (0.87)	0.89 7.726 7.741	-0.015						
t45g30m2	7.130 (0.54)	0.59 7.134 7.167	-0.033	7.430 (1.07)	1.15 7.432 7.466	-0.034	7.730 (2.04)	2.19 7.728 7.763	-0.035						
t45g20m2	7.130 (1.26)	1.41 7.127 7.185	-0.058	7.430 (2.40)	2.69 7.425 7.487	-0.062	7.730 (4.47)	5.01 7.726 7.794	-0.068						
t45g10m2	7.130 (3.02)	3.55 7.132 7.208	-0.076	7.430 (5.50)	6.46 7.425 7.509	-0.084	7.730 (9.77)	11.48 7.730 7.827	-0.097						
t65g50m3	6.130 (0.60)	0.66 6.126 6.169	-0.043	6.430 (1.20)	1.32 6.431 6.474	-0.043	6.730 (2.34)	2.57 6.729 6.774	-0.045						
t65g40m3	6.130 (1.32)	1.62 6.127 6.224	-0.097	6.430 (2.57)	3.16 6.428 6.528	-0.100	6.730 (4.90)	6.03 6.726 6.832	-0.106						
t65g30m3	6.130 (2.69)	3.98 6.132 6.311	-0.179	6.430 (5.13)	7.59 6.431 6.620	-0.189	6.730 (9.55)	14.13 6.733 6.936	-0.203						
t65g20m3	6.130 (5.13)	9.12 6.126 6.402	-0.276	6.430 (9.77)	16.98 6.426 6.728	-0.302	6.730 (16.98)	30.20 6.736 7.075	-0.339						
t65g10m3	6.130 (9.55)	18.20 6.126 6.463	-0.337	6.430 (16.98)	32.36 6.430 6.809	-0.379	6.730 (28.84)	52.48 6.727 7.177	-0.450						
t60g50m3	6.130 (0.28)	0.30 6.135 6.164	-0.029	6.430 (0.55)	0.59 6.427 6.456	-0.029	6.730 (1.10)	1.17 6.731 6.761	-0.030						
t60g40m3	6.130 (0.62)	0.71 6.125 6.191	-0.066	6.430 (1.20)	1.41 6.431 6.498	-0.067	6.730 (2.34)	2.75 6.731 6.800	-0.069						
t60g30m3	6.130 (1.38)	1.78 6.131 6.246	-0.115	6.430 (2.63)	3.47 6.435 6.554	-0.119	6.730 (5.01)	6.46 6.727 6.855	-0.128						
t60g20m3	6.130 (2.95)	4.17 6.125 6.296	-0.171	6.430 (5.50)	7.94 6.429 6.613	-0.184	6.730 (10.00)	14.45 6.729 6.928	-0.199						
t60g10m3	6.130 (5.75)	9.12 6.129 6.359	-0.230	6.430 (10.47)	16.60 6.426 6.673	-0.247	6.730 (18.20)	28.84 6.731 7.013	-0.282						
t55g50m3	6.130 (0.11)	0.11 6.131 6.148	-0.017	6.430 (0.22)	0.23 6.430 6.448	-0.018	6.730 (0.44)	0.46 6.732 6.750	-0.018						
t55g40m3	6.130 (0.25)	0.27 6.127 6.169	-0.042	6.430 (0.49)	0.54 6.429 6.472	-0.043	6.730 (0.95)	1.07 6.734 6.777	-0.043						
t55g30m3	6.130 (0.58)	0.69 6.133 6.211	-0.078	6.430 (1.12)	1.35 6.429 6.509	-0.080	6.730 (2.19)	2.63 6.732 6.816	-0.084						
t55g20m3	6.130 (1.29)	1.66 6.130 6.238	-0.108	6.430 (2.51)	3.24 6.429 6.541	-0.112	6.730 (4.79)	6.17 6.730 6.850	-0.120						
t55g10m3	6.130 (2.88)	3.89 6.131 6.275	-0.144	6.430 (5.37)	7.41 6.435 6.586	-0.151	6.730 (9.77)	13.49 6.733 6.901	-0.168						
t50g50m3	6.130 (0.03)	0.03 6.130 6.143	-0.013	6.430 (0.07)	0.07 6.431 6.443	-0.012	6.730 (0.13)	0.13 6.729 6.743	-0.014						
t50g40m3	6.130 (0.08)	0.09 6.127 6.155	-0.028	6.430 (0.16)	0.17 6.429 6.457	-0.028	6.730 (0.32)	0.34 6.730 6.759	-0.029						
t50g30m3	6.130 (0.18)	0.21 6.127 6.186	-0.059	6.430 (0.36)	0.42 6.429 6.489	-0.060	6.730 (0.72)	0.83 6.733 6.793	-0.060						
t50g20m3	6.130 (0.45)	0.54 6.132 6.215	-0.083	6.430 (0.87)	1.05 6.427 6.511	-0.084	6.730 (1.70)	2.04 6.727 6.815	-0.088						
t50g10m3	6.130 (1.15)	1.41 6.135 6.223	-0.088	6.430 (2.24)	2.69 6.426 6.518	-0.092	6.730 (4.17)	5.13 6.728 6.826	-0.098						
t45g50m3	6.130 (0.01)	0.01 6.127 6.135	-0.008	6.430 (0.01)	0.01 6.426 6.434	-0.008	6.730 (0.03)	0.03 6.725 6.734	-0.009						
t45g40m3	6.130 (0.02)	0.02 6.124 6.146	-0.022	6.430 (0.04)	0.04 6.425 6.447	-0.022	6.730 (0.07)	0.08 6.726 6.748	-0.022						
t45g30m3	6.130 (0.05)	0.05 6.126 6.165	-0.039	6.430 (0.10)	0.10 6.432 6.471	-0.039	6.730 (0.19)	0.21 6.733 6.771	-0.038						
t45g20m3	6.130 (0.11)	0.13 6.126 6.194	-0.068	6.430 (0.23)	0.26 6.426 6.495	-0.069	6.730 (0.45)	0.52 6.729 6.798	-0.069						
t45g10m3	6.130 (0.31)	0.36 6.126 6.198	-0.072	6.430 (0.62)	0.72 6.430 6.503	-0.073	6.730 (1.20)	1.41 6.728 6.803	-0.075						

NOTE — The case of $\xi = 2 \text{ km s}^{-1}$ calculation for the middle line of the infrared oxygen triplet, O I 7774.17. Code “*taagbbmc*” denotes the model with $T_{\text{eff}} = aa \times 100$, $\log g = bb/10$, and $[\text{Fe}/\text{H}]$ (metallicity) = $-c$. Calculations for each model were made three times corresponding to three assigned oxygen abundances, A_i^{a} ($\equiv 8.93 + [\text{Fe}/\text{H}] + [\text{O}/\text{Fe}]_i$) ($i = 1, 2, 3$), where $([\text{O}/\text{Fe}]_1, [\text{O}/\text{Fe}]_2, [\text{O}/\text{Fe}]_3)$ are $(-0.3, 0.0, +0.3)$ for the solar metallicity models ($[\text{Fe}/\text{H}] = 0$) and $(+0.2, +0.5, +0.8)$ for all other metal-deficient models ($[\text{Fe}/\text{H}] = -1, -2, -3$). W_i^{LTE} and W_i^{NLTE} are the resulting theoretical LTE and NLTE equivalent widths (in mÅ) corresponding to the assigned A_i^{a} , respectively. Based on such calculated *non-LTE* equivalent width, W_i^{NLTE} , two kinds of oxygen abundances were inversely computed for the cases of NLTE (A_i^{N}) and LTE (A_i^{L}), from which the *non-LTE* abundance correction was eventually evaluated as the difference of these two, Δ_i ($\equiv A_i^{\text{N}} - A_i^{\text{L}}$).

Table 3: Coefficients (a , b) for O I 7771.94.

T_{eff}	$\log g$	a ($\xi = 1$)	b ($\xi = 1$)	W range	a ($\xi = 2$)	b ($\xi = 2$)	W range	a ($\xi = 3$)	b ($\xi = 3$)	W range
4500	1.0	-0.075002	0.009542	(1, 65)	-0.075356	0.008023	(1, 74)	-0.074381	0.006728	(1, 85)
4500	2.0	-0.063934	0.009469	(0, 41)	-0.063630	0.008285	(0, 46)	-0.063137	0.006891	(0, 52)
4500	3.0	-0.035192	0.011033	(0, 27)	-0.034745	0.011525	(0, 28)	-0.034471	0.009788	(0, 30)
4500	4.0	-0.017092	0.007009	(0, 15)	-0.016955	0.007648	(0, 16)	-0.017007	0.006311	(0, 17)
4500	5.0	-0.007669	-0.012856	(0, 8)	-0.007191	-0.014193	(0, 8)	-0.006915	-0.013005	(0, 8)
5000	1.0	-0.107305	0.006369	(2,135)	-0.107536	0.005386	(2,155)	-0.106370	0.004483	(2,182)
5000	2.0	-0.093306	0.007027	(1, 96)	-0.093021	0.005981	(1,110)	-0.092000	0.005021	(1,126)
5000	3.0	-0.060149	0.008351	(0, 66)	-0.060438	0.007135	(0, 74)	-0.059794	0.006105	(0, 83)
5000	4.0	-0.026452	0.010508	(0, 44)	-0.026505	0.009854	(0, 48)	-0.026579	0.008254	(0, 52)
5000	5.0	-0.010772	0.007419	(0, 31)	-0.010895	0.006636	(0, 32)	-0.010664	0.006359	(0, 34)
5500	1.0	-0.173154	0.004333	(5,200)	-0.171278	0.003712	(5,234)	-0.168826	0.003108	(5,282)
5500	2.0	-0.130188	0.005075	(2,162)	-0.129085	0.004355	(2,186)	-0.127260	0.003656	(2,219)
5500	3.0	-0.088392	0.005886	(1,123)	-0.088652	0.005063	(1,138)	-0.087546	0.004300	(1,158)
5500	4.0	-0.045400	0.006999	(0, 89)	-0.045010	0.006242	(0, 98)	-0.044836	0.005401	(0,110)
5500	5.0	-0.017273	0.007421	(0, 66)	-0.017193	0.006644	(0, 71)	-0.017248	0.005989	(0, 76)
6000	1.0	-0.266939	0.003000	(13,251)	-0.260351	0.002631	(12,295)	-0.247962	0.002325	(13,347)
6000	2.0	-0.199517	0.003669	(6,214)	-0.196006	0.003214	(6,245)	-0.191289	0.002757	(6,288)
6000	3.0	-0.129293	0.004429	(3,174)	-0.128434	0.003859	(2,200)	-0.126288	0.003282	(3,234)
6000	4.0	-0.069964	0.005137	(1,138)	-0.070334	0.004515	(1,155)	-0.068899	0.003922	(1,178)
6000	5.0	-0.029232	0.005318	(0,112)	-0.028856	0.004924	(0,120)	-0.029252	0.004288	(0,132)
6500	1.0	-0.425820	0.002043	(25,282)	-0.406389	0.001874	(25,331)	-0.382757	0.001703	(25,389)
6500	2.0	-0.316286	0.002456	(13,251)	-0.305817	0.002219	(13,295)	-0.291792	0.001979	(13,347)
6500	3.0	-0.198270	0.003252	(6,219)	-0.195040	0.002890	(6,251)	-0.187683	0.002557	(6,288)
6500	4.0	-0.106599	0.003996	(2,182)	-0.104490	0.003609	(2,204)	-0.102594	0.003146	(2,234)
6500	5.0	-0.044660	0.004404	(1,155)	-0.045000	0.003978	(1,170)	-0.044197	0.003590	(1,186)

NOTE — The coefficients (a , b) used with the analytic formula [Eq.(1)] for evaluating the non-LTE correction, corresponding to each of the atmospheric models (T_{eff} and $\log g$ values shown in columns 1 and 2) for three values of the microturbulent velocity ($\xi = 1, 2$, and 3 km s^{-1}). The “ W range” gives the minimum and the maximum value of the equivalent-width data (in mÅ) based on which the coefficients were established (i.e., indication of the range of the W_λ values to which the formula with these coefficients can be applied).

Table 4: Coefficients (a , b) for O I 7774.17.

T_{eff}	$\log g$	a ($\xi = 1$)	b ($\xi = 1$)	W range	a ($\xi = 2$)	b ($\xi = 2$)	W range	a ($\xi = 3$)	b ($\xi = 3$)	W range
4500	1.0	-0.073793	0.010148	(0, 58)	-0.073780	0.008488	(0, 66)	-0.072979	0.007092	(0, 76)
4500	2.0	-0.063712	0.006132	(0, 35)	-0.062821	0.008346	(0, 40)	-0.062356	0.006906	(0, 45)
4500	3.0	-0.035064	0.010989	(0, 23)	-0.034614	0.011527	(0, 23)	-0.034347	0.009430	(0, 26)
4500	4.0	-0.016938	0.007280	(0, 13)	-0.017033	0.005749	(0, 13)	-0.016773	0.004774	(0, 14)
4500	5.0	-0.007297	-0.010223	(0, 6)	-0.006829	-0.012540	(0, 6)	-0.007200	-0.023415	(0, 7)
5000	1.0	-0.105560	0.006706	(1,123)	-0.105520	0.005653	(1,141)	-0.104210	0.004709	(1,166)
5000	2.0	-0.091507	0.007408	(1, 87)	-0.091394	0.006292	(1, 98)	-0.090448	0.005256	(1,112)
5000	3.0	-0.059339	0.008759	(0, 58)	-0.059182	0.007595	(0, 65)	-0.058655	0.006327	(0, 72)
5000	4.0	-0.026360	0.010633	(0, 37)	-0.026406	0.009823	(0, 41)	-0.026522	0.008324	(0, 45)
5000	5.0	-0.010885	0.006427	(0, 26)	-0.010977	0.005904	(0, 26)	-0.010598	0.005227	(0, 28)
5500	1.0	-0.168793	0.004559	(4,191)	-0.166332	0.003922	(4,219)	-0.163428	0.003289	(4,257)
5500	2.0	-0.126021	0.005383	(2,148)	-0.125805	0.004568	(2,170)	-0.124542	0.003804	(2,200)
5500	3.0	-0.087354	0.006180	(1,110)	-0.086594	0.005325	(1,123)	-0.085991	0.004476	(1,141)
5500	4.0	-0.044505	0.007448	(0, 78)	-0.044722	0.006527	(0, 85)	-0.044613	0.005536	(0, 96)
5500	5.0	-0.016934	0.007810	(0, 56)	-0.017195	0.006915	(0, 60)	-0.017136	0.006154	(0, 65)
6000	1.0	-0.254642	0.003237	(9,240)	-0.243609	0.002897	(9,275)	-0.236696	0.002478	(9,331)
6000	2.0	-0.192306	0.003910	(4,200)	-0.189738	0.003393	(4,229)	-0.185979	0.002875	(4,269)
6000	3.0	-0.125586	0.004661	(2,162)	-0.124640	0.004046	(2,182)	-0.122884	0.003402	(2,214)
6000	4.0	-0.068886	0.005361	(1,126)	-0.068406	0.004741	(1,138)	-0.067629	0.004055	(1,155)
6000	5.0	-0.028857	0.005626	(0, 96)	-0.028811	0.005050	(0,105)	-0.028577	0.004510	(0,112)
6500	1.0	-0.390958	0.002323	(19,269)	-0.375496	0.002093	(18,316)	-0.356457	0.001876	(19,372)
6500	2.0	-0.294824	0.002727	(9,240)	-0.285213	0.002443	(9,275)	-0.272451	0.002166	(9,324)
6500	3.0	-0.189861	0.003492	(4,204)	-0.185155	0.003121	(4,229)	-0.181040	0.002675	(4,269)
6500	4.0	-0.101634	0.004302	(2,166)	-0.101045	0.003789	(2,186)	-0.099058	0.003275	(2,214)
6500	5.0	-0.043878	0.004657	(1,138)	-0.043743	0.004213	(1,148)	-0.043188	0.003693	(1,166)

NOTE — See the caption of table 3 for the meanings of the columns.

Table 5: Coefficients (a , b) for O I 7775.39.

T_{eff}	$\log g$	a ($\xi = 1$)	b ($\xi = 1$)	W range	a ($\xi = 2$)	b ($\xi = 2$)	W range	a ($\xi = 3$)	b ($\xi = 3$)	W range
4500	1.0	-0.071843	0.010860	(0, 48)	-0.071891	0.009057	(0, 55)	-0.070976	0.007520	(0, 62)
4500	2.0	-0.061323	0.009180	(0, 29)	-0.060937	0.008329	(0, 32)	-0.060347	0.006721	(0, 36)
4500	3.0	-0.034389	0.010752	(0, 18)	-0.033807	0.010977	(0, 18)	-0.033636	0.008536	(0, 20)
4500	4.0	-0.016737	0.002727	(0, 10)	-0.016927	0.000833	(0, 10)	-0.016618	0.001652	(0, 10)
4500	5.0	-0.010138	-0.096676	(0, 4)	-0.010362	-0.095794	(0, 4)	-0.009923	-0.090568	(0, 4)
5000	1.0	-0.102353	0.007223	(1,107)	-0.102838	0.006040	(1,123)	-0.101612	0.005036	(1,141)
5000	2.0	-0.089035	0.007937	(0, 72)	-0.089088	0.006640	(0, 83)	-0.088580	0.005489	(0, 93)
5000	3.0	-0.058042	0.008875	(0, 47)	-0.058165	0.007677	(0, 52)	-0.057643	0.006315	(0, 59)
5000	4.0	-0.025786	0.011203	(0, 30)	-0.026091	0.009942	(0, 32)	-0.025790	0.008631	(0, 35)
5000	5.0	-0.010567	0.006446	(0, 19)	-0.010740	0.004815	(0, 20)	-0.010665	0.003706	(0, 20)
5500	1.0	-0.161349	0.004926	(2,170)	-0.160227	0.004180	(2,195)	-0.158235	0.003473	(2,229)
5500	2.0	-0.121987	0.005726	(1,129)	-0.122434	0.004800	(1,148)	-0.120899	0.003995	(1,170)
5500	3.0	-0.084362	0.006543	(0, 93)	-0.084568	0.005556	(0,105)	-0.083895	0.004600	(0,117)
5500	4.0	-0.043955	0.007729	(0, 63)	-0.044054	0.006737	(0, 69)	-0.043452	0.005682	(0, 76)
5500	5.0	-0.017604	-0.001526	(0, 44)	-0.017034	0.006931	(0, 47)	-0.017098	0.006145	(0, 49)
6000	1.0	-0.230850	0.003678	(6,219)	-0.226046	0.003208	(6,251)	-0.220972	0.002705	(6,302)
6000	2.0	-0.182907	0.004231	(3,178)	-0.182280	0.003577	(3,209)	-0.179144	0.003005	(3,240)
6000	3.0	-0.120395	0.004954	(1,141)	-0.120003	0.004222	(1,158)	-0.118602	0.003513	(1,182)
6000	4.0	-0.066570	0.005688	(0,105)	-0.066206	0.004914	(0,115)	-0.065479	0.004137	(0,129)
6000	5.0	-0.027805	0.006041	(0, 78)	-0.027918	0.005307	(0, 83)	-0.028125	0.004557	(0, 91)
6500	1.0	-0.348779	0.002725	(12,251)	-0.337745	0.002434	(12,288)	-0.328159	0.002095	(12,347)
6500	2.0	-0.266789	0.003117	(6,219)	-0.260165	0.002749	(6,251)	-0.252698	0.002368	(6,295)
6500	3.0	-0.178059	0.003805	(3,182)	-0.175237	0.003326	(2,204)	-0.172827	0.002783	(2,240)
6500	4.0	-0.096075	0.004634	(1,141)	-0.096248	0.003982	(1,158)	-0.094877	0.003362	(1,182)
6500	5.0	-0.042435	0.004943	(0,112)	-0.042258	0.004382	(0,123)	-0.041729	0.003805	(0,135)

NOTE — See the caption of table 3 for the meanings of the columns.

Table 6: $[\text{O}/\text{Fe}]$ ratio averaged for each metallicity bin.

Metallicity Range	n_{77}	$\langle[\text{O}/\text{Fe}]_{77}\rangle$	σ_{77}	n_{63}	$\langle[\text{O}/\text{Fe}]_{63}\rangle$	σ_{63}	$\langle[\text{O}/\text{Fe}]_{77}\rangle - \langle[\text{O}/\text{Fe}]_{63}\rangle$
$-2.75 \leq [\text{Fe}/\text{H}] < -2.25$	25	+0.90	0.19	11	+0.58	0.15	+0.32
$-2.25 \leq [\text{Fe}/\text{H}] < -1.75$	26	+0.80	0.21	17	+0.46	0.18	+0.34
$-1.75 \leq [\text{Fe}/\text{H}] < -1.25$	35	+0.69	0.24	29	+0.47	0.18	+0.22
$-1.25 \leq [\text{Fe}/\text{H}] < -0.75$	32	+0.55	0.23	10	+0.45	0.23	+0.10
$-0.75 \leq [\text{Fe}/\text{H}] < -0.25$	54	+0.26	0.16	17	+0.18	0.23	+0.03
$-0.25 \leq [\text{Fe}/\text{H}] < +0.25$	28	-0.04	0.12	10	+0.14	0.16	-0.18

NOTE — n_{77} and n_{63} are the numbers of stars used for calculating $\langle[\text{O}/\text{Fe}]_{77}\rangle$ and $\langle[\text{O}/\text{Fe}]_{63}\rangle$ at each metallicity bin, while σ_{77} and σ_{63} are the standard deviations.

Table 7: NLTE abundance correction for the O I 6158.2 line ($\xi = 2 \text{ km s}^{-1}$).

Code	A_1^a (W_1^{LTE})	W_1^{NLTE}	A_1^{N}	A_1^{L}	Δ_1	A_2^a (W_2^{LTE})	W_2^{NLTE}	A_2^{N}	A_2^{L}	Δ_2	A_3^a (W_3^{LTE})	W_3^{NLTE}	A_3^{N}	A_3^{L}	Δ_3
t65g50m0	8.630 (5.62)	5.62	8.633	8.633	0.000	8.930 (10.47)	10.47	8.928	8.928	0.000	9.230 (19.05)	18.62	9.225	9.224	0.001
t65g40m0	8.630 (10.47)	10.72	8.628	8.637	-0.009	8.930 (18.20)	18.62	8.932	8.941	-0.009	9.230 (29.51)	30.20	9.232	9.242	-0.010
t65g30m0	8.630 (17.38)	19.05	8.636	8.680	-0.044	8.930 (28.18)	30.20	8.927	8.979	-0.052	9.230 (42.66)	45.71	9.230	9.293	-0.063
t65g20m0	8.630 (32.36)	36.31	8.633	8.705	-0.072	8.930 (48.98)	53.70	8.924	9.018	-0.094	9.230 (67.61)	75.86	9.231	9.353	-0.122
t65g10m0	8.630 (44.67)	52.48	8.621	8.775	-0.154	8.930 (61.66)	75.86	8.938	9.146	-0.208	9.230 (81.28)	100.00	9.232	9.491	-0.259
t60g50m0	8.630 (2.63)	2.63	8.635	8.634	0.001	8.930 (5.01)	5.01	8.934	8.933	0.001	9.230 (9.12)	9.12	9.227	9.225	0.002
t60g40m0	8.630 (5.13)	5.13	8.628	8.631	-0.003	8.930 (9.33)	9.33	8.933	8.936	-0.003	9.230 (15.85)	15.85	9.231	9.234	-0.003
t60g30m0	8.630 (9.33)	9.77	8.632	8.654	-0.022	8.930 (15.85)	16.60	8.937	8.962	-0.025	9.230 (25.12)	25.70	9.222	9.252	-0.030
t60g20m0	8.630 (15.85)	18.20	8.635	8.712	-0.077	8.930 (25.12)	28.18	8.923	9.017	-0.094	9.230 (37.15)	42.66	9.239	9.353	-0.114
t60g10m0	8.630 (29.51)	33.88	8.634	8.729	-0.095	8.930 (43.65)	50.12	8.936	9.059	-0.123	9.230 (60.26)	69.18	9.233	9.387	-0.154
t55g50m0	8.630 (1.05)	1.05	8.629	8.628	0.001	8.930 (2.04)	2.04	8.931	8.930	0.001	9.230 (3.89)	3.89	9.234	9.232	0.002
t55g40m0	8.630 (2.19)	2.19	8.625	8.625	0.000	8.930 (4.07)	4.07	8.926	8.926	0.000	9.230 (7.24)	7.24	9.225	9.225	0.000
t55g30m0	8.630 (4.17)	4.27	8.627	8.638	-0.011	8.930 (7.41)	7.59	8.927	8.939	-0.012	9.230 (12.59)	12.88	9.235	9.248	-0.013
t55g20m0	8.630 (8.13)	8.71	8.635	8.675	-0.040	8.930 (13.49)	14.45	8.935	8.981	-0.046	9.230 (20.89)	22.39	9.229	9.285	-0.056
t55g10m0	8.630 (14.13)	16.22	8.632	8.720	-0.088	8.930 (21.88)	25.70	8.937	9.047	-0.110	9.230 (32.36)	37.15	9.222	9.355	-0.133
t50g50m0	8.630 (0.32)	0.32	8.625	8.624	0.001	8.930 (0.63)	0.63	8.932	8.931	0.001	9.230 (1.23)	1.23	9.234	9.232	0.002
t50g40m0	8.630 (0.74)	0.74	8.626	8.626	0.000	8.930 (1.45)	1.45	8.936	8.935	0.001	9.230 (2.63)	2.63	9.229	9.228	0.001
t50g30m0	8.630 (1.58)	1.62	8.634	8.639	-0.005	8.930 (2.95)	2.95	8.928	8.934	-0.006	9.230 (5.13)	5.25	9.235	9.240	-0.005
t50g20m0	8.630 (3.39)	3.47	8.626	8.645	-0.019	8.930 (5.75)	6.03	8.934	8.955	-0.021	9.230 (9.33)	9.77	9.233	9.258	-0.025
t50g10m0	8.630 (6.17)	6.61	8.624	8.669	-0.045	8.930 (10.23)	11.22	8.934	8.988	-0.054	9.230 (16.22)	17.38	9.226	9.287	-0.061
t45g50m0	8.630 (0.05)	0.05	8.635	8.633	0.002	8.930 (0.09)	0.09	8.931	8.930	0.001	9.230 (0.18)	0.18	9.226	9.225	0.001
t45g40m0	8.630 (0.16)	0.16	8.627	8.626	0.001	8.930 (0.32)	0.32	8.926	8.925	0.001	9.230 (0.62)	0.62	9.232	9.231	0.001
t45g30m0	8.630 (0.40)	0.40	8.631	8.633	-0.002	8.930 (0.76)	0.76	8.930	8.932	-0.002	9.230 (1.41)	1.41	9.235	9.236	-0.001
t45g20m0	8.630 (0.91)	0.93	8.629	8.640	-0.011	8.930 (1.70)	1.74	8.931	8.943	-0.012	9.230 (3.02)	3.09	9.232	9.245	-0.013
t45g10m0	8.630 (1.91)	2.00	8.628	8.650	-0.022	8.930 (3.39)	3.55	8.930	8.955	-0.025	9.230 (5.75)	6.03	9.237	9.266	-0.029
t65g50m1	8.130 (1.29)	1.29	8.134	8.128	0.006	8.430 (2.51)	2.51	8.431	8.426	0.005	8.730 (4.90)	4.79	8.725	8.720	0.005
t65g40m1	8.130 (2.82)	2.82	8.127	8.128	-0.001	8.430 (5.37)	5.37	8.428	8.429	-0.001	8.730 (9.77)	9.77	8.726	8.726	0.000
t65g30m1	8.130 (5.89)	6.31	8.135	8.166	-0.031	8.430 (10.47)	11.22	8.431	8.466	-0.035	8.730 (17.78)	19.05	8.735	8.775	-0.040
t65g20m1	8.130 (12.59)	13.80	8.132	8.178	-0.046	8.430 (21.38)	23.44	8.429	8.484	-0.055	8.730 (33.88)	37.15	8.729	8.798	-0.069
t65g10m1	8.130 (19.50)	22.91	8.128	8.227	-0.099	8.430 (31.62)	37.15	8.429	8.553	-0.124	8.730 (46.77)	54.95	8.722	8.878	-0.156
t60g50m1	8.130 (0.51)	0.50	8.129	8.123	0.006	8.430 (1.00)	1.00	8.434	8.428	0.006	8.730 (1.95)	1.95	8.732	8.725	0.007
t60g40m1	8.130 (1.15)	1.12	8.130	8.124	0.006	8.430 (2.19)	2.19	8.433	8.426	0.007	8.730 (4.17)	4.07	8.725	8.718	0.007
t60g30m1	8.130 (2.57)	2.63	8.130	8.139	-0.009	8.430 (4.79)	4.90	8.429	8.439	-0.010	8.730 (8.71)	8.71	8.725	8.735	-0.010
t60g20m1	8.130 (5.37)	5.89	8.129	8.180	-0.051	8.430 (9.55)	10.47	8.427	8.485	-0.058	8.730 (15.85)	17.78	8.734	8.805	-0.071
t60g10m1	8.130 (11.48)	12.88	8.134	8.193	-0.059	8.430 (19.05)	21.38	8.427	8.497	-0.070	8.730 (30.20)	33.88	8.736	8.822	-0.086
t55g50m1	8.130 (0.18)	0.18	8.134	8.129	0.005	8.430 (0.35)	0.35	8.435	8.430	0.005	8.730 (0.71)	0.69	8.728	8.723	0.005
t55g40m1	8.130 (0.41)	0.40	8.132	8.124	0.008	8.430 (0.79)	0.78	8.428	8.419	0.009	8.730 (1.55)	1.51	8.729	8.720	0.009
t55g30m1	8.130 (0.91)	0.89	8.126	8.122	0.004	8.430 (1.74)	1.74	8.432	8.427	0.005	8.730 (3.31)	3.24	8.729	8.724	0.005
t55g20m1	8.130 (2.04)	2.14	8.133	8.150	-0.017	8.430 (3.80)	3.98	8.433	8.451	-0.018	8.730 (6.76)	7.08	8.732	8.753	-0.021
t55g10m1	8.130 (4.37)	4.90	8.131	8.186	-0.055	8.430 (7.76)	8.71	8.430	8.492	-0.062	8.730 (13.18)	14.79	8.734	8.807	-0.073
t50g50m1	8.130 (0.05)	0.05	8.132	8.129	0.003	8.430 (0.11)	0.11	8.429	8.426	0.003	8.730 (0.21)	0.21	8.732	8.729	0.003
t50g40m1	8.130 (0.13)	0.13	8.129	8.123	0.006	8.430 (0.26)	0.25	8.430	8.424	0.006	8.730 (0.50)	0.49	8.725	8.719	0.006
t50g30m1	8.130 (0.28)	0.28	8.126	8.118	0.008	8.430 (0.55)	0.55	8.434	8.426	0.008	8.730 (1.07)	1.05	8.725	8.717	0.008
t50g20m1	8.130 (0.65)	0.65	8.133	8.134	-0.001	8.430 (1.23)	1.23	8.427	8.427	0.000	8.730 (2.34)	2.34	8.732	8.732	0.000
t50g10m1	8.130 (1.48)	1.55	8.128	8.147	-0.019	8.430 (2.82)	2.95	8.435	8.455	-0.020	8.730 (5.01)	5.25	8.727	8.750	-0.023
t45g50m1	8.130 (0.01)	0.01	8.153	8.151	0.002	8.430 (0.01)	0.01	8.420	8.419	0.001	8.730 (0.03)	0.03	8.722	8.720	0.002
t45g40m1	8.130 (0.03)	0.03	8.139	8.135	0.004	8.430 (0.05)	0.05	8.431	8.427	0.004	8.730 (0.11)	0.11	8.733	8.729	0.004
t45g30m1	8.130 (0.07)	0.07	8.128	8.121	0.007	8.430 (0.14)	0.14	8.430	8.423	0.007	8.730 (0.28)	0.28	8.733	8.727	0.006
t45g20m1	8.130 (0.17)	0.17	8.135	8.133	0.002	8.430 (0.32)	0.32	8.431	8.429	0.002	8.730 (0.63)	0.63	8.731	8.728	0.003
t45g10m1	8.130 (0.41)	0.42	8.128	8.137	-0.009	8.430 (0.79)	0.81	8.430	8.440	-0.010	8.730 (1.51)	1.55	8.732	8.742	-0.010

Note — The case of $\xi = 2 \text{ km s}^{-1}$ calculation (only on the $[\text{Fe}/\text{H}] = 0$ and -1 models) for the O I 6158.2 line comprising three components. See the note in Table 2 for more details.

Fig. 1.— Non-LTE correction vs. equivalent-width relation calculated for O I 7774.17 (the middle line of the oxygen triplet) with the microturbulent velocity (ξ) of 2 km s^{-1} , as constructed from $(W_i^{\text{NLTE}}, \Delta_i)$ given in Table 2. Results corresponding to each of the models are discerned by differences in symbols. (a): high gravity cases ($\log g = 5.0, 4.0,$ and 3.0); (b): low gravity cases ($\log g = 3.0, 2.0,$ and 1.0).

Fig. 2.— Error of the analytical expression for the non-LTE correction (O I 7774.17, $\xi = 2 \text{ km s}^{-1}$), $\Delta \log \epsilon = a10^{bW_\lambda}$ with the coefficients (a, b) given in Table 4, relative to the exactly calculated value (Table 2, Figure 1). Similarly to Figure 1, the results are shown as functions of W_λ .

Fig. 3.— Comparison of the non-LTE abundance corrections derived in previous two works of the author, with those calculated by our analytical formula using appropriate (a, b) coefficients evaluated by interpolating the values in Tables 3–5. (a): O I 7771.94 in population I G–K giants (Takeda et al. 1998); (b): O I 7771–5 in very metal-poor giants (Takeda et al. 2000).

Fig. 4.— Comparison of our non-LTE abundance corrections for O I 7771–5 triplet resulting from reanalysis of the published equivalent-width data by use of our approximate analytical formula with the original values determined by those authors. (a): Tomkin et al. (1992); (b): Mishenina et al. (2000).

Fig. 5.— (a): Comparison of our non-LTE abundance corrections for O I 7771–5 triplet resulting from reanalysis of the data of Tomkin et al. (1992) and Edvardsson et al. (1993) (as was done by Carretta et al. 2000) with the corrections determined by Carretta et al. (2000). (b): Differences between Carretta et al’s (2000) non-LTE corrections and ours, plotted as functions of metallicity.

Fig. 6.— Non-LTE correction vs. equivalent-width relation calculated by Gratton et al. (1999) for O I 7771.94 (large symbols) and our relevant (metallicity-independent) analytical relation (solid line; which was determined so as to fit the original data shown by the small open circles). (a): $T_{\text{ef}} = 5000 \text{ K}$, $\log g = 3.0$; (b): $T_{\text{ef}} = 6000 \text{ K}$, $\log g = 3.0$.

Fig. 7.— (a): $[\text{O}/\text{Fe}]$ vs. $[\text{Fe}/\text{H}]$ relation based on the reanalysis of published equivalent width data of O I 7771–5 lines (closed symbols, half-filled symbols, crosses) and [O I] 6300/6363 lines (open symbols), where the non-LTE correction was taken into account only for the O I triplet lines. The solid and dashed lines indicate the mean $[\text{O}/\text{Fe}]$ tendencies suggested from permitted O I lines and forbidden [O I] lines, respectively. (b): Applied non-LTE corrections for the O I 7771–5 lines plotted with respect to the metallicity.

Each of the symbols denote the sources of equivalent widths. O I 7771–5: filled squares—Carretta et al. (2000), St. Andrew’s crosses—Edvardsson et al. (1993), filled inverse triangles—Abia & Rebolo (1989), Greek Crosses—Boesgaard & King (1993), half-filled triangles—Sneden et al. (1979), filled triangles—Mishenina et al. (2000), filled diamonds—Tomkin et al. (1992), filled circles—Cavallo et al. (1997), half-filled circles—Takeda et al. (2000), half-filled square—King (1994). [O I] 6300/6363: open squares—Carretta et al. (2000), open inverse triangles—Sneden et al. (1979), open triangles—Mishenina et al. (2000), open diamonds—Barbuy (1988) and Barbuy & Erdelyi-Mendes (1989),

open circles—Snedden et al. (1991) and Kraft et al. (1992), open stars—Takeda et al. (2000)

Fig. 8.— Dependence of $[\text{O}/\text{Fe}]_{7771-5} - \langle [\text{O}/\text{Fe}]_{6300/6363} \rangle$ (the discrepancy of each star’s $[\text{O}/\text{Fe}]_{7771-5}$ relative to the mean $\langle [\text{O}/\text{Fe}]_{6300/6363} \rangle$) upon (a) T_{eff} and (b) $\log g$. Filled symbols are for stars of $-2.75 \leq [\text{Fe}/\text{H}] < -2.25$, while closed symbols correspond to those of $-2.25 \leq [\text{Fe}/\text{H}] < -1.75$.

Fig. 9.— Dependence of $[\text{O}/\text{Fe}]_{6300/6363} - \langle [\text{O}/\text{Fe}]_{7771-5} \rangle$ upon (a) T_{eff} and (b) $\log g$. The rather isolated point at high T_{eff} (5755 K) and high $\log g$ (3.66) corresponds to HD 140283, the $W_\lambda(6300)$ data (0.5 mÅ) for which was taken from Carretta et al. (2000). Otherwise, the same as in Figure 8.

Fig. 10.— Dependence of the non-LTE correction for the O I 7774.18 line upon the logarithmic correction (h) applied to the classical treatment of H I collision rates. Left panel: ($[\text{O}/\text{Fe}] = 0.0$, $\xi = 2 \text{ km s}^{-1}$) calculations for representative $[\text{Fe}/\text{H}] = 0$ models; right panel: ($[\text{O}/\text{Fe}] = +0.5$, $\xi = 2 \text{ km s}^{-1}$) calculations for representative $[\text{Fe}/\text{H}] = -2$ models. See the note in Table 2 for the meaning of the code given each model in the figure.

Fig. 11.— Comparison of the oxygen abundances derived from the O I 7771–5 lines (with the NLTE corrections presented in this study) with those determined from other oxygen lines for nearby solar-type stars analyzed by Takeda et al. (2001): (a) O I 6158.2 line (comprising three components), (b) [O I] 6300 forbidden line.

Fig. 12.— Results of the calculations on the simple “two-level atom plus continuum” model for simulating the formation of the O I 7771–5 triplet. Shown are the results computed for three different combinations of B_1 (gradient of the Planck function) and e' (photon destruction probability) as indicated in the figure. (a) Theoretical curves of growth computed for LTE (without scattering) and NLTE (with scattering). (b) Run of the non-LTE correction ($\equiv \log \eta_{\text{NLTE}} - \log \eta_{\text{LTE}}$) with the NLTE equivalent width.

Figure 1

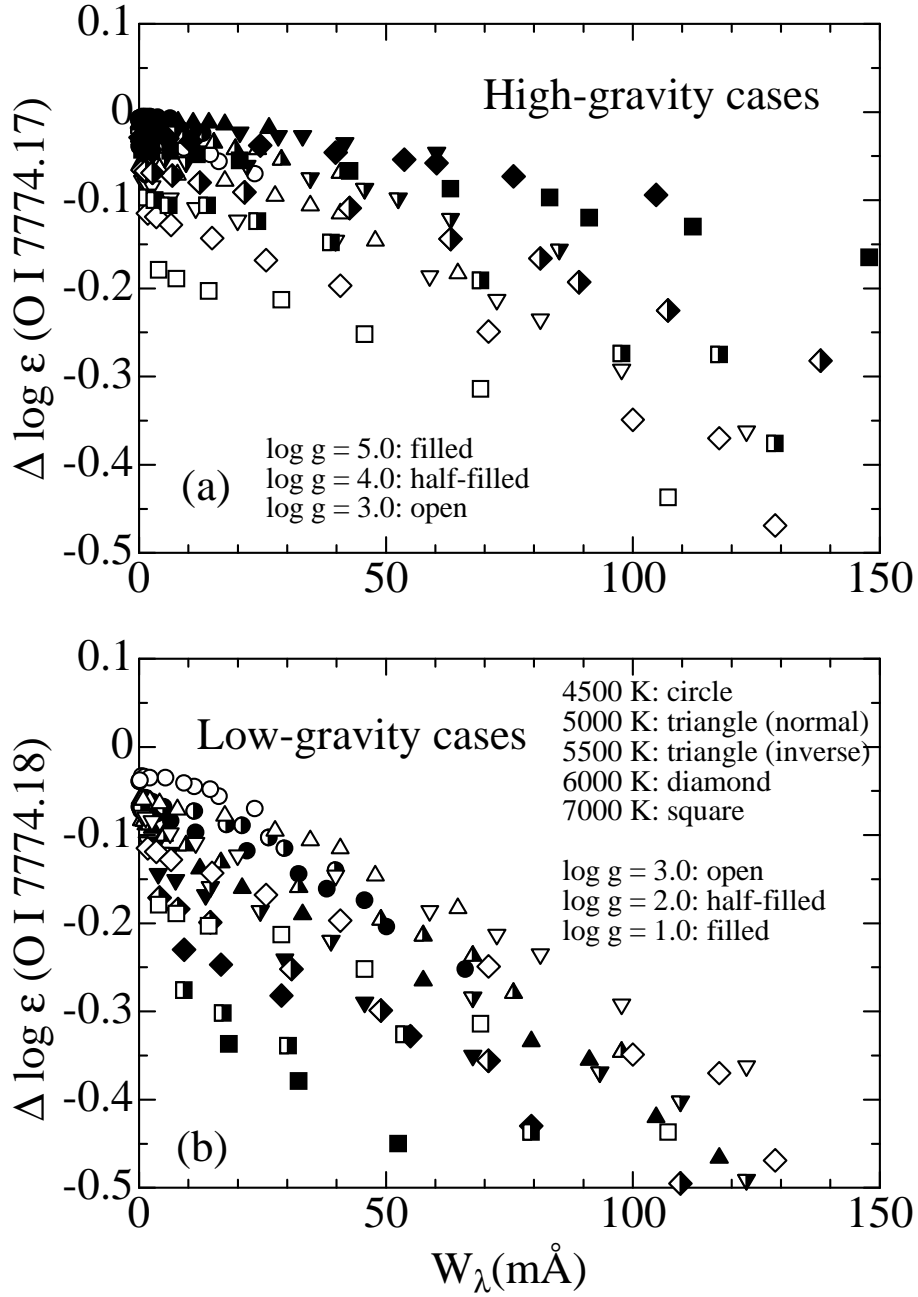


Figure 2

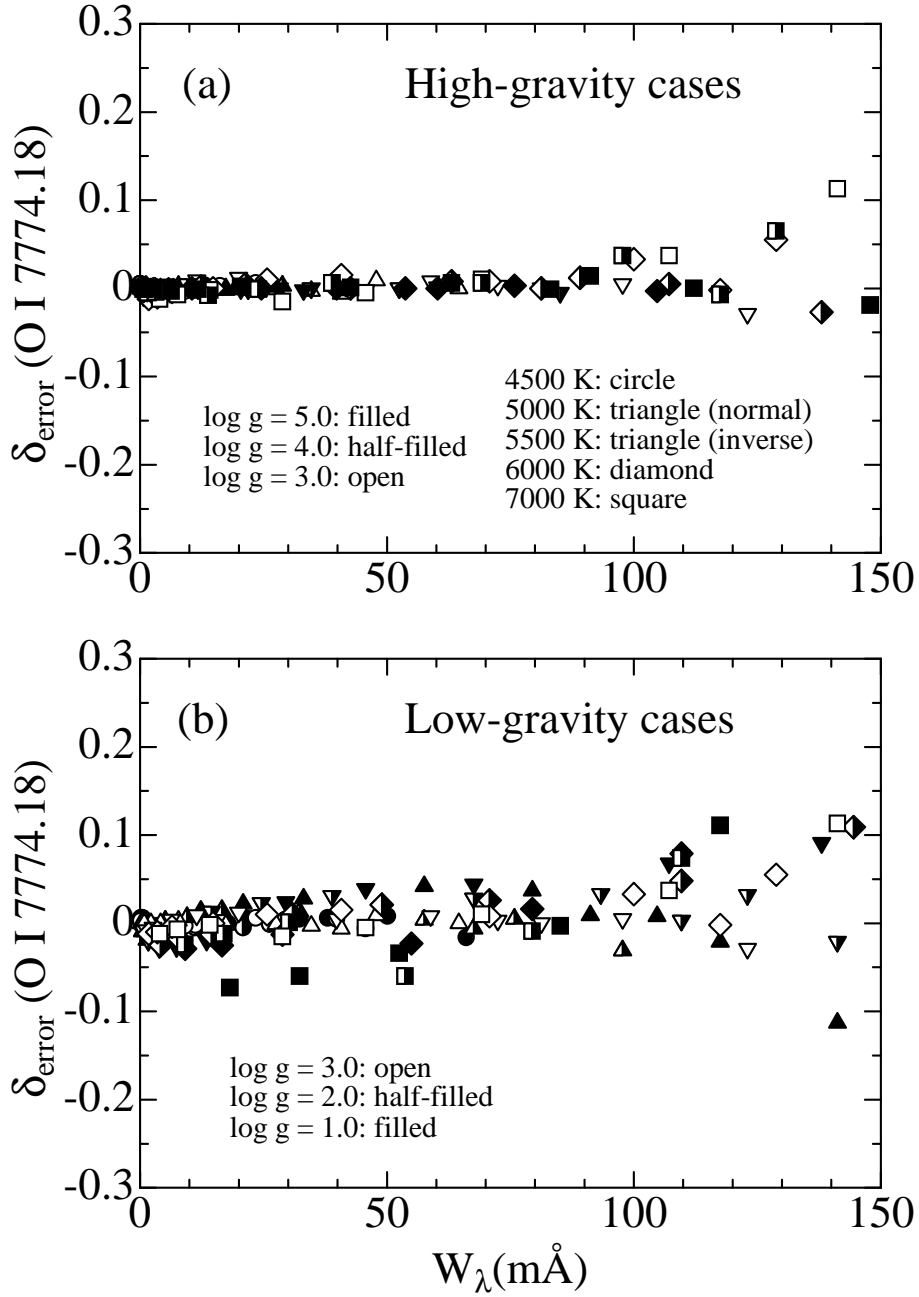


Figure 3

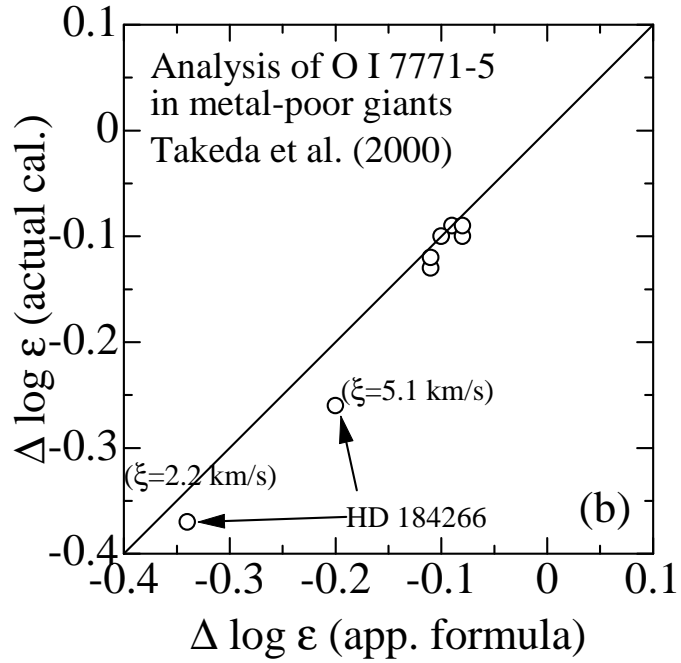
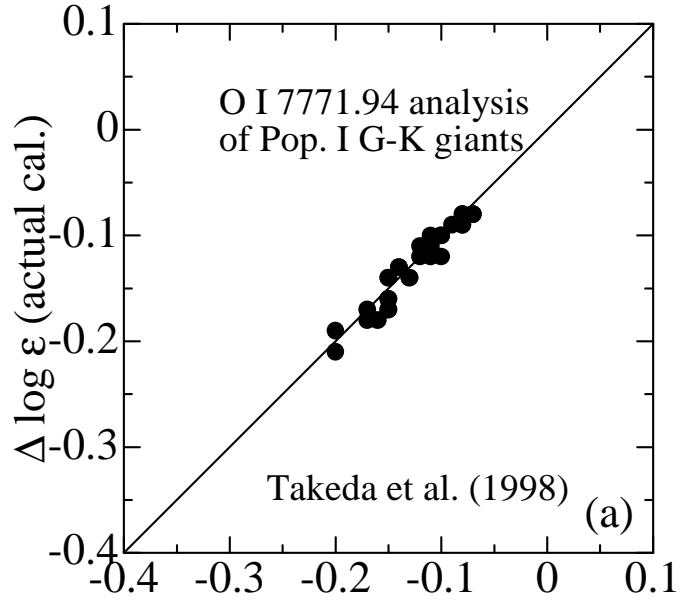


Figure 4

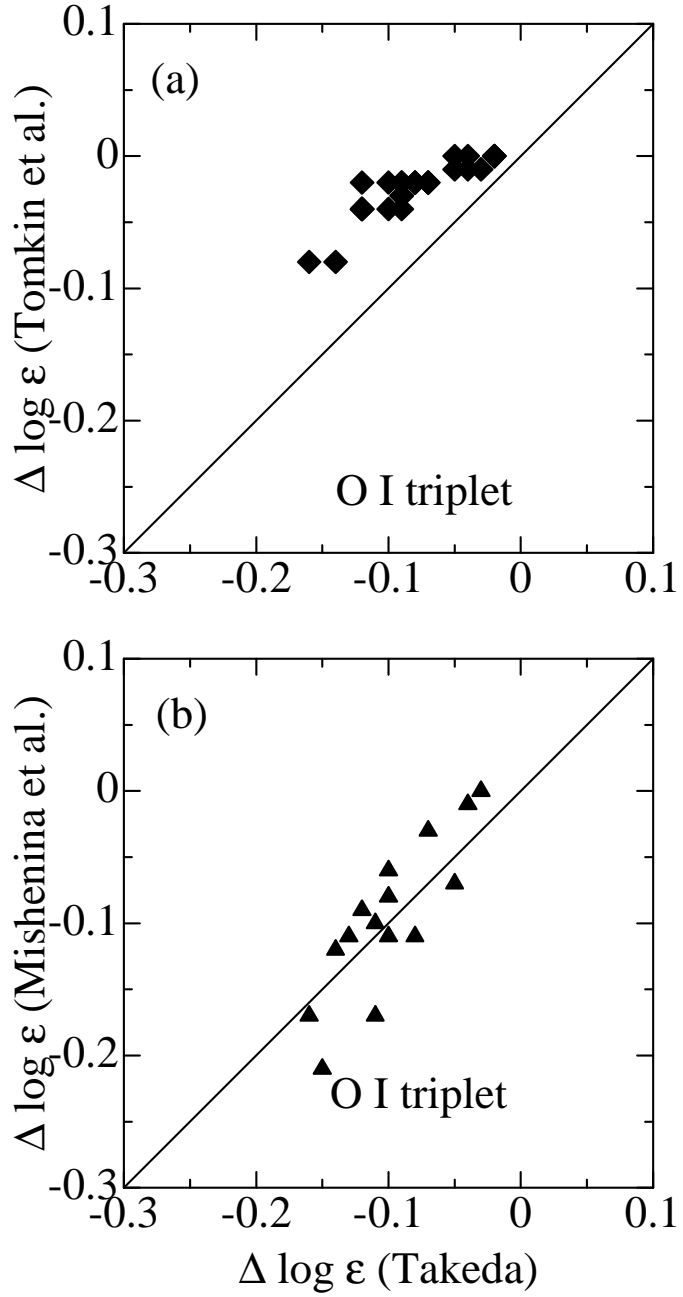


Figure 5

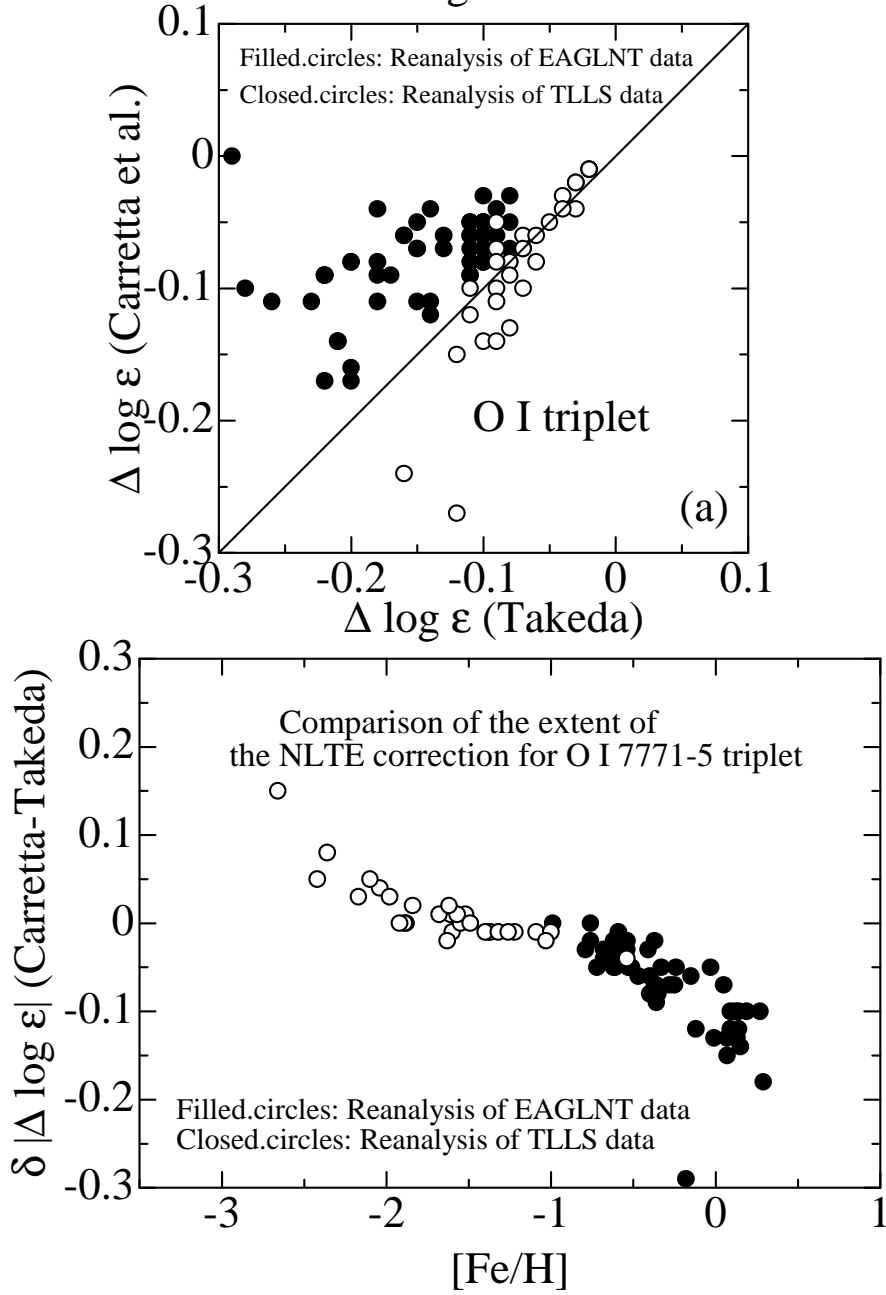


Figure 6

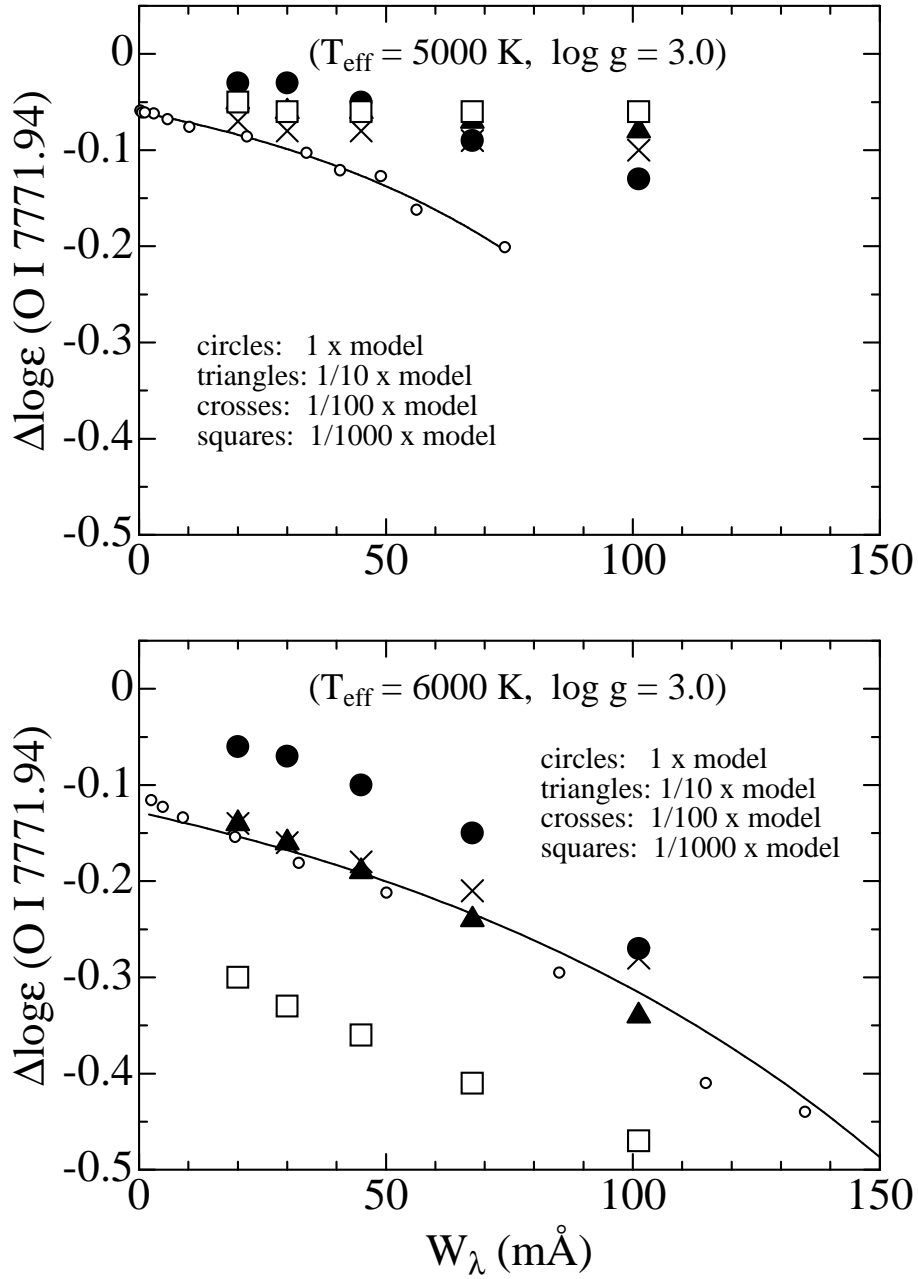


Figure 7

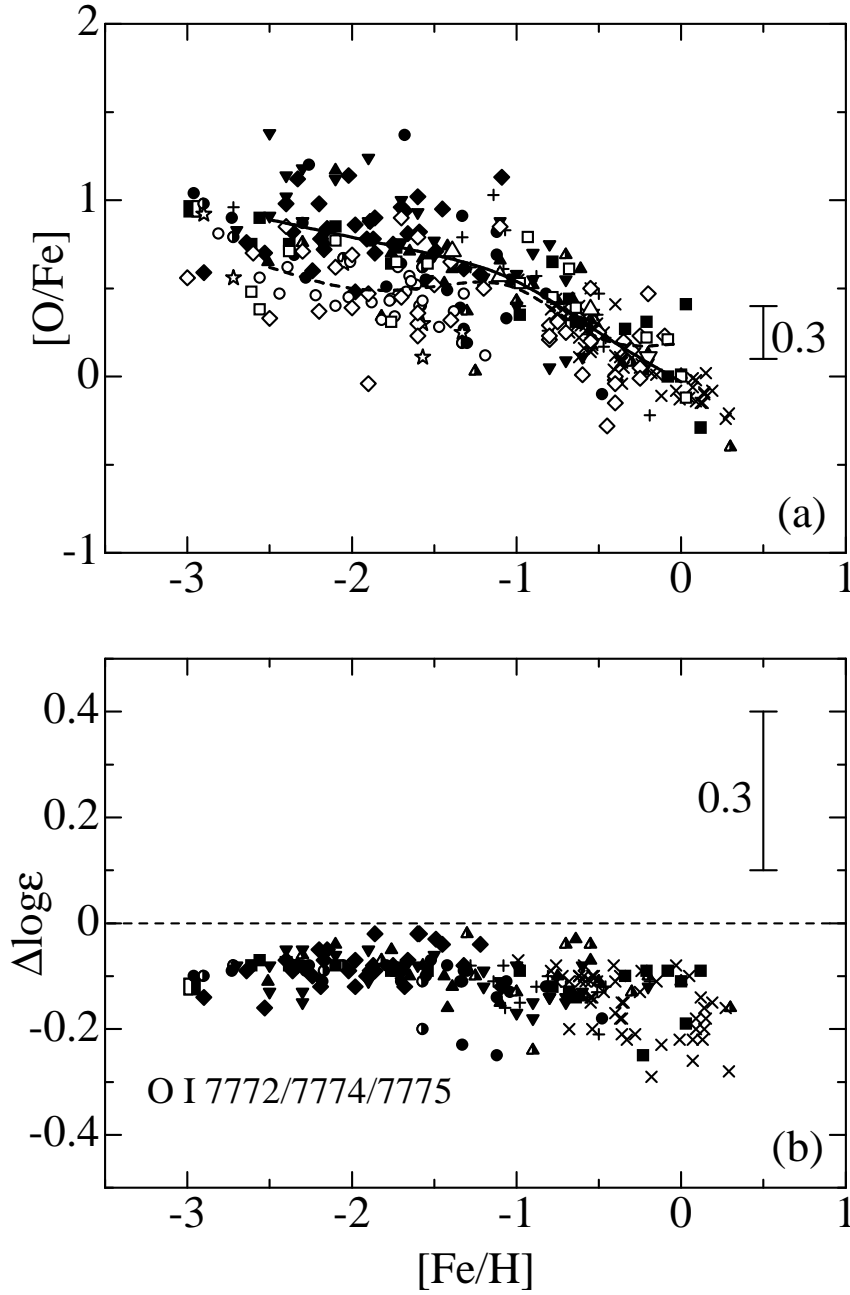


Figure 8

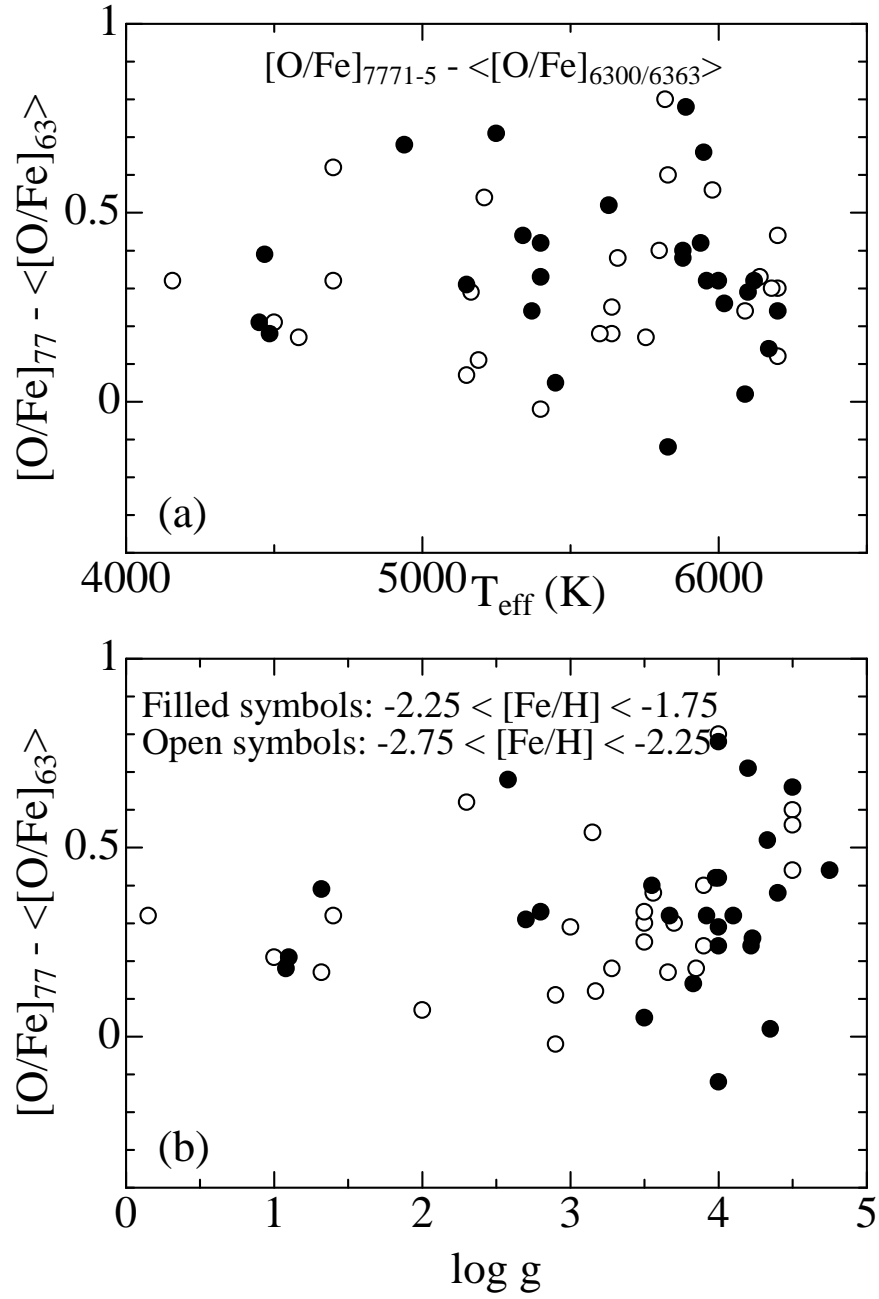


Figure 9

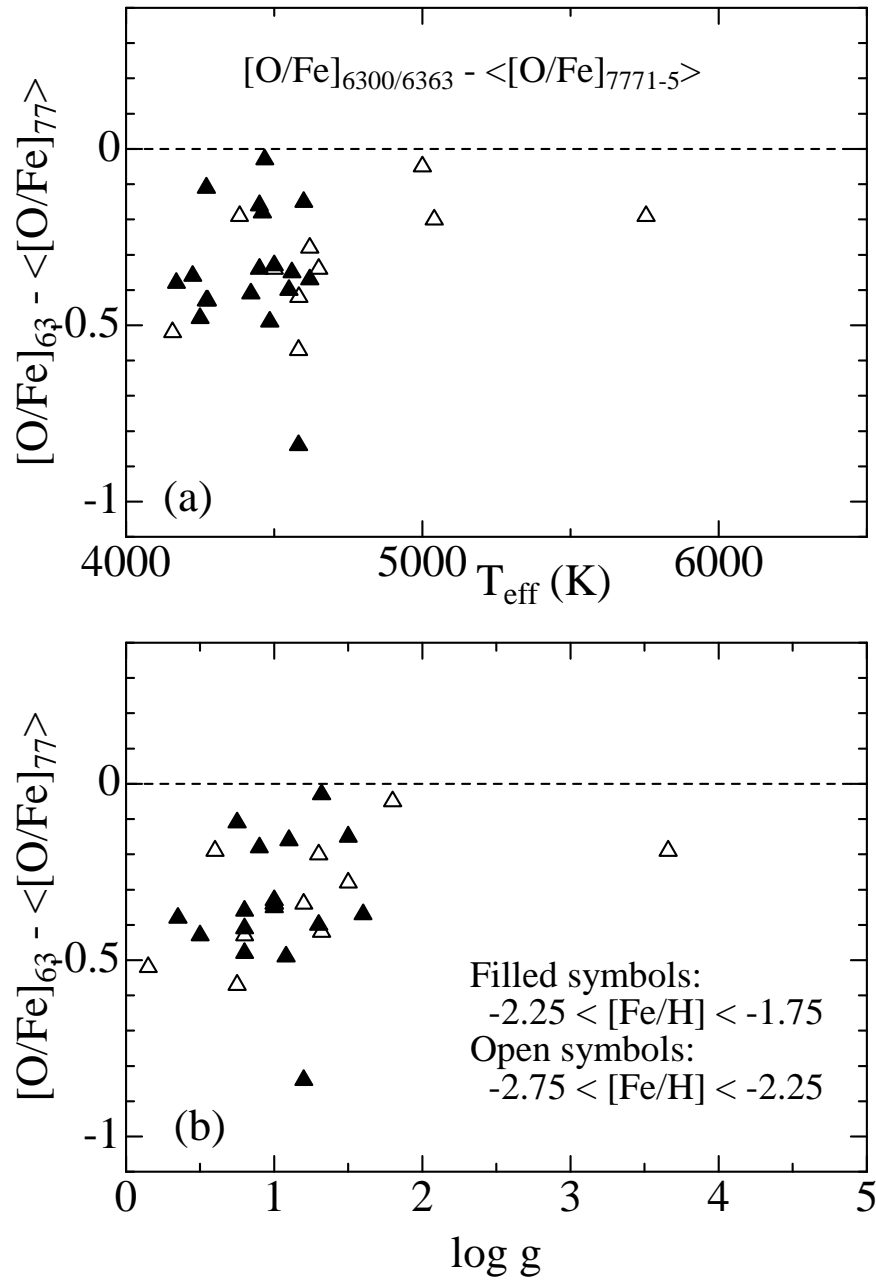


Figure 10

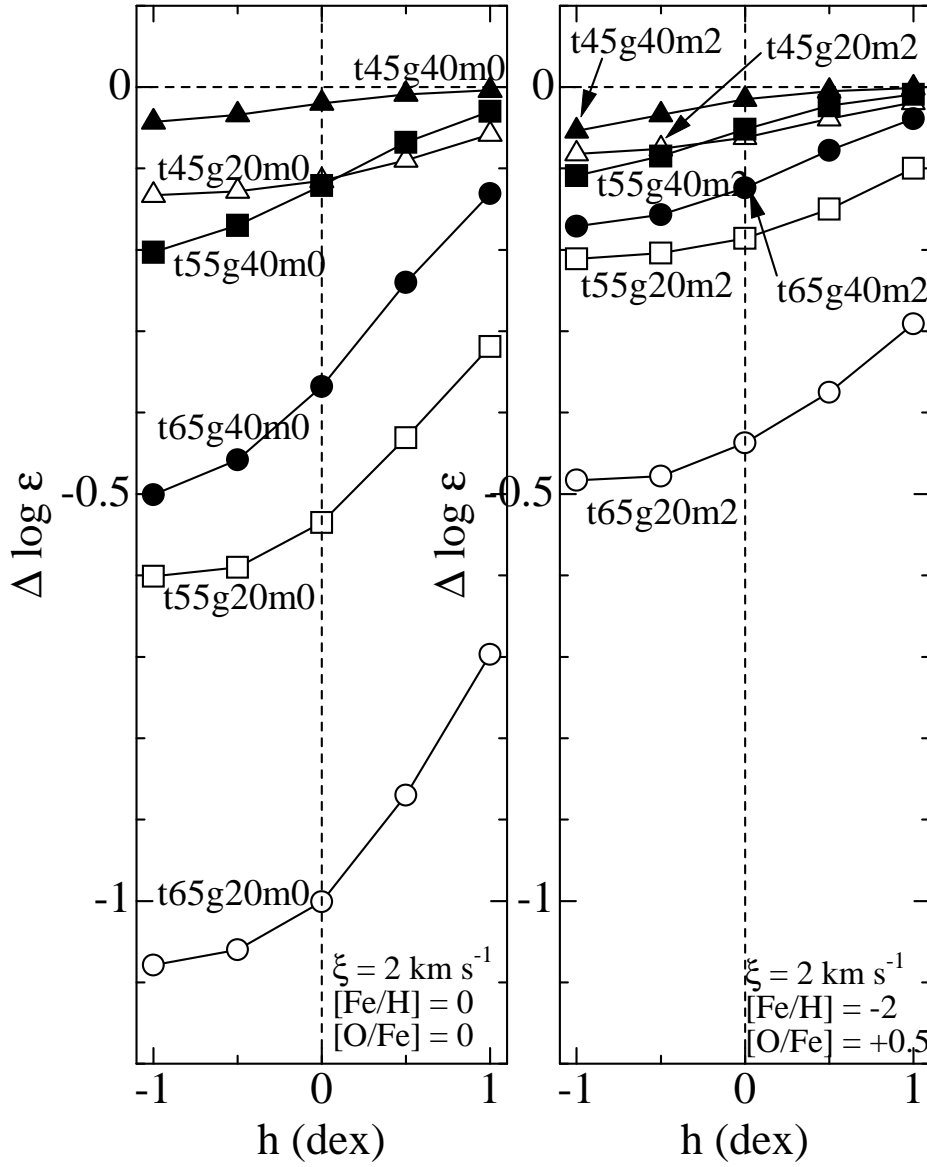


Figure 11

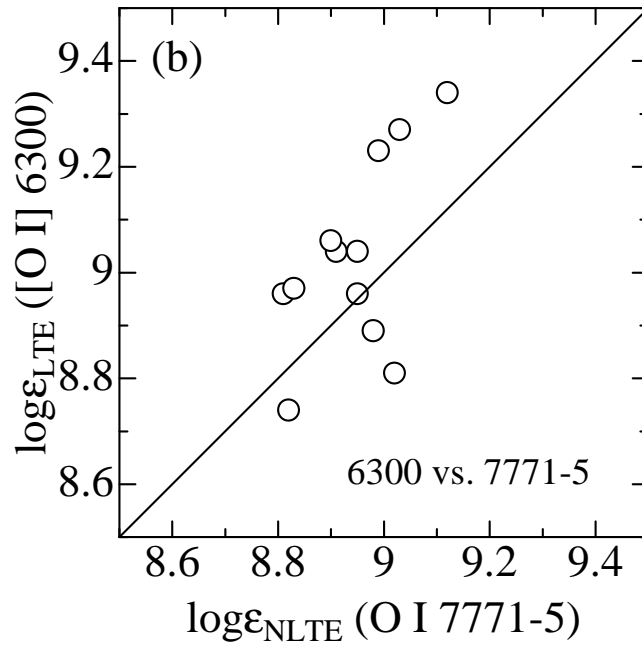
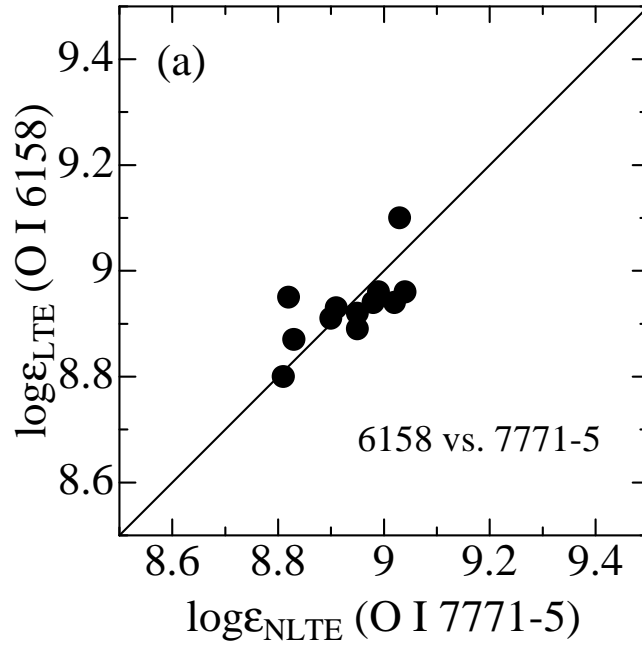


Figure 12

